Ultrafast dynamics of hot carriers: Theoretical approaches based on real-time propagation of carrier distributions

Jelena Sjakste, Raja Sen, Nathalie Vast, Jérôme Saint-Martin, Mohammad Ghanem, Philippe Dollfus, Felipe Murphy-Armando, Junichi Kanasaki

The Journal of Chemical Physics

AIP Publishing

Ultrafast dynamics of hot carriers: Theoretical approaches based on real-time propagation of carrier distributions.

Jelena Sjakste,[1] Raja Sen,[2] Nathalie Vast,[1] Jerome Saint-Martin,[3] Mohammad Ghanem,[4] Philippe Dollfus,[4] Felipe Murphy-Armando,[5] and Junichi Kanasaki[6]

[1)] *Laboratoire des Solides Irradies, CEA/DRF/IRAMIS, Ecole Polytechnique, CNRS, Institut Polytechnique de Paris, 91120 Palaiseau, France*

[2)] *Sorbonne Université, Museum National d'Histoire Naturelle, UMR CNRS 7590, Institut de Minéralogie, de Physique des Matériaux et de Cosmochimie, 4 place Jussieu, F-75005 Paris, France*

[3)] *SATIE, CNRS, ENS Paris-Saclay, Université Paris-Saclay, 91190 Gif-sur-Yvette, France*

[4)] *Université Paris-Saclay, CNRS, Centre de Nanosciences et de Nanotechnologies, 91120, Palaiseau, France*

[5)] *Tyndall National Institute, University College Cork, T12R5CP, Ireland*

[6)] *Department of Mechanical Engineering, Graduate school of Engineering, Osaka Metropolitan University, 1-1 Gakuen-cho, Naka-ku, Sakai, Osaka 599-8531, Japan*

(Dated: 21 January 2025)

In recent years, computational approaches which couple density functional theory (DFT) - based description of the electron-phonon and phonon-phonon scattering rates with the Boltzmann transport equation have been shown to obtain the electron and thermal transport characteristics of many 3D and 2D semiconductors in excellent agreement with experimental measurements. At the same time, progress in the DFT-based description of the electron-phonon scattering has also allowed to describe the non-equilibrium relaxation dynamics of hot or photo-excited electrons in several materials, in very good agreement with time-resolved spectroscopy experiments. In the latter case, as the time-resolved spectroscopy techniques provide the possibility to monitor transient material characteristics evolving on the femtosecond and attosecond time scales, the time evolution of photo-excited, nonthermal carrier distributions has to be described. Similarly, reliable theoretical approaches are needed to describe the transient transport properties of devices involving high energy carriers.

In this review, we aim to discuss recent progress in coupling the *ab initio* description of materials, especially that of the electron-phonon scattering, with the time-dependent approaches describing the time evolution of the out-of-equilibrium carrier distributions, in the context of time-resolved spectroscopy experiments as well as in the context of transport simulations. We point out the computational limitations common to all numerical approaches which describe time propagation of strongly out-of-equilibrium carrier distributions in 3D materials, and discuss the methods used to overcome them.

I. INTRODUCTION

In recent years, spectacular progress has been achieved in the *ab initio* density functional theory (DFT) - based description of electronic and thermal transport in solids. Today, methods based on DFT allow the calculation of electron-phonon and phonon-phonon scattering rates from first principles[1–3], whereas carrier and thermal transport characteristics of many 3D and 2D semiconductors are well described within the approaches which couple DFT with the Boltzmann transport equations (BTEs) .[4–11]. At the same time, progress in the DFT-based description of the electron-phonon scattering also allowed to describe the relaxation dynamics of hot or photo-excited electrons in several materials in very good agreement with time-resolved spectroscopy experiments[2,12–16]. In the latter case, however, the theoretical approaches which couple the DFT description of materials with the *stationary* BTE, in which the time derivative of carrier distributions is not considered, are often insufficient. Instead, one has to describe the time evolution of photo-excited, nonthermal carrier distributions[13,17]. Indeed, time-resolved spectroscopy techniques, such as time- and angle-resolved photoemission spectroscopy as well as phase-resolved transient absorption spectroscopy, provide the possibility to monitor *transient* material characteristics which are due to photo-excited carrier distributions evolving on femtosecond and attosecond time scales[18–28]. At the same time, future generations of energy converters might involve high energy carriers, therefore requiring reliable theoretical approaches to describe the *transient* transport properties of devices[29–32].

In this review, we aim to discuss recent progress in coupling the *ab initio* description of materials, especially that of the electron-phonon scattering, with the time-dependent approaches describing the time evolution of the out-of-equilibrium carrier distributions, in the context of time-resolved spectroscopy experiments as well as in the context of transport simulations.

We start (Section II) by the discussion of the out-of-equilibrium carrier distributions in energy and momentum spaces, and of the main mechanisms leading to the equilibration of carrier distributions with respect to their energy and momentum, on competing timescales. In Section III we discuss the electron-phonon scattering as the main mechanism which determines the relaxation dynamics of photo-excited electrons, and provide a brief overview of the most widely-used DFT-based methods to calculate the electron-phonon scattering matrix

elements[1,8,33], as well as of some important and recent developments[34,35]. In Section IV we introduce time-dependent coupled Boltzmann transport equations for electrons and phonons, and discuss recent developments towards the fully *ab initio* momentum-resolved time propagation of the hot or photo-excited carrier distributions[7,36,37]. We then describe less general approaches, such as the concept of hot electron ensemble[15,16,18], which led to significant progress in the understanding of time-resolved photoemission experiments in several semiconductors (Section V), and time propagation of hot thermal carrier distributions beyond the two-temperature model in the context of time-resolved diffuse scattering experiments (Section VI)[12,14]. Then in Section VII, we discuss recent attempts to apply non-adiabatic molecular dynamics (NAMD) approaches to photo-excited carrier relaxation dynamics in semiconductors[38–40]. Finally, in Section VIII, we turn to the context of transport and discuss the propagation in time of carrier distributions using the stochastic Monte Carlo (MC) approach[41–43], showing that MC approaches coupled with DFT descriptions of scattering mechanisms are well-suited to calculating photo-excited carrier relaxation dynamics. We conclude by a brief discussion of computational limitations common to all numerical approaches which describe time propagation of strongly out-of-equilibrium carrier distributions in energy and momentum spaces for 3D materials, the paths to overcome them currently being explored, and finally, end with a discussion of perspectives and open questions.

II. RELAXATION REGIMES AND CARRIER DISTRIBUTIONS

When the excitation of charge carriers occurs much faster than typical relaxation timescales, which are usually of the order of tens of femtoseconds to a few picoseconds, the system enters an ultra-fast transient transport regime during which time dependent non-equilibrium processes occur.[44] In electronic devices, this transport regime typically arises immediately after electric or magnetic fields, or temperature gradients, are switched on. This regime precedes the stationary regime in which the flux and density of carriers are constant in time. However, the final stationary regime of a continuously excited system may still involve the transfer of energy from carriers to phonons.

In the literature about spectroscopy in the ultra-fast regime, the photo-excited carrier relaxation is usually classified into four temporally overlapping regimes: the coherent regime, non-thermal regime, hot-carrier regime and isothermal regime[45–47]. In the non-thermal

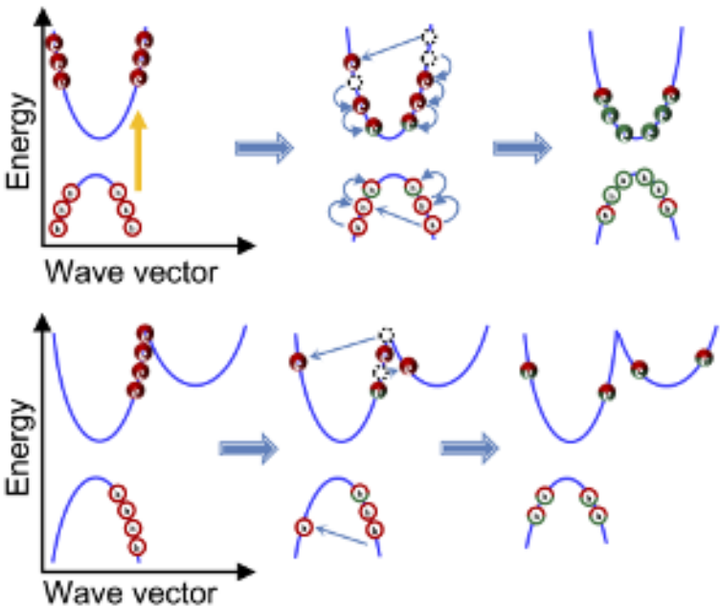

FIG. 1. Schematic representation of the quasi-equilibration processes for photo-excited carrier distributions in a semiconductor, at time scales ranging from few fs to few ps. Full/empty circles represent photo-excited electrons/holes. Red color corresponds to out-of-equilibrium carriers, green to equilibrium ones. Upper panel: Quasi-equilibration of carrier distributions with respect to energy. From left to right: initial non-thermal carrier distribution created by a laser pulse; thermalization process via electron-electron and electron-phonon coupling; quasi-thermalized "hot" distribution, continuing to cool via electron-phonon scattering. Lower panel: Quasi-equilibration of carrier distributions, with respect to their momentum. From left to right: Initial out-of-equilibrium carrier distribution created by a laser pulse, populating only one of the available valleys in one particular direction in the Brillouin Zone; equilibration in momentum space, due to intervalley and intravalley electron-phonon scattering; distribution quasi-equilibrated in momentum space.

regime, carrier distributions differ strongly from the Fermi-Dirac distribution, whereas in the hot-carrier regime, carriers can be described by a thermal distribution with however a temperature higher than that of the lattice. All scattering processes such as electron-phonon, electron-electron and electron-impurity scattering can contribute to all of the above-mentioned regimes[28,47–54], apart from the isothermal regime, in which excited electrons and holes recombine. Nevertheless, it is generally understood that the electron-electron scattering mainly affects early stages after photo-excitation, playing an important role in decoher-

ence and thermalization of carriers[28,50,55–60], whereas electron-phonon scattering is the main driver which governs the cooling of hot electrons[13,17,61–63] (see e.g. Ref. 47 for a detailed discussion).

A. Energy distributions

The above-described different regimes of carrier relaxation involve different types of out-of-equilibrium carrier distributions that are based on their *energy*: Non-thermal carrier distributions at early stages, transitioning to thermal but still "hot" carrier distributions later on, are schematically presented in the upper panel of Fig. 1. As an example, highly non-thermal distributions created by a photo-excitation with a *s*-polarised 3.59 eV light in silicon from Ref. 18 are shown in Fig. 2. In this work[18], normal photoemission spectra of photo-excited silicon was probed by a *p*-polarised 4.67 eV light at Δt =10 fs and Δt =450 fs after photo-excitation. As one can see from Fig. 2, the electronic distributions are highly non-thermal at Δt =10 fs (shown by blue curves). The photo-excited electrons then thermalize at the bottom of the lowest valley of the conduction band (CB) within few hundreds of fs[18,64,65], as illustrated by the red curves for Δt =450 fs in Fig. 2.

Theoretically, the initial distribution of photo-excited carriers produced by ultrafast laser pulses on attosecond time scales can be studied by from-first-principles methods based on the DFT[66], such as Time Dependent Density Functional Theory (TDDFT) and related methods[67–77], as well as theoretical methods beyond TDDFT[78–83]. Those methods, however, are computationally demanding. Thus, in some theoretical works, to solely focus on the relaxation dynamics (as opposed to excitation and decoherence dynamics), the initial highly non-thermal distributions were approximated by a Gaussian function or a superposition of several Gaussian functions[36,43,62,84,85].

In contrast to non-thermal distributions, the "hot", or quasi-thermalized carrier distribution f^{th} can be described analytically and reads as follows[50,86]:

$$f^{th} = \frac{1}{1 + exp(\frac{\varepsilon - E_f^*}{k_B T_e})} \tag{1}$$

where T_e is the electronic temperature, ε is the carrier energy, E_f^* is the quasi-Fermi level. Note than the latter can differ considerably from the final thermal equilibrium Fermi level E_f, as very hot electrons (holes) can potentially thermalize in upper local minima (valleys)

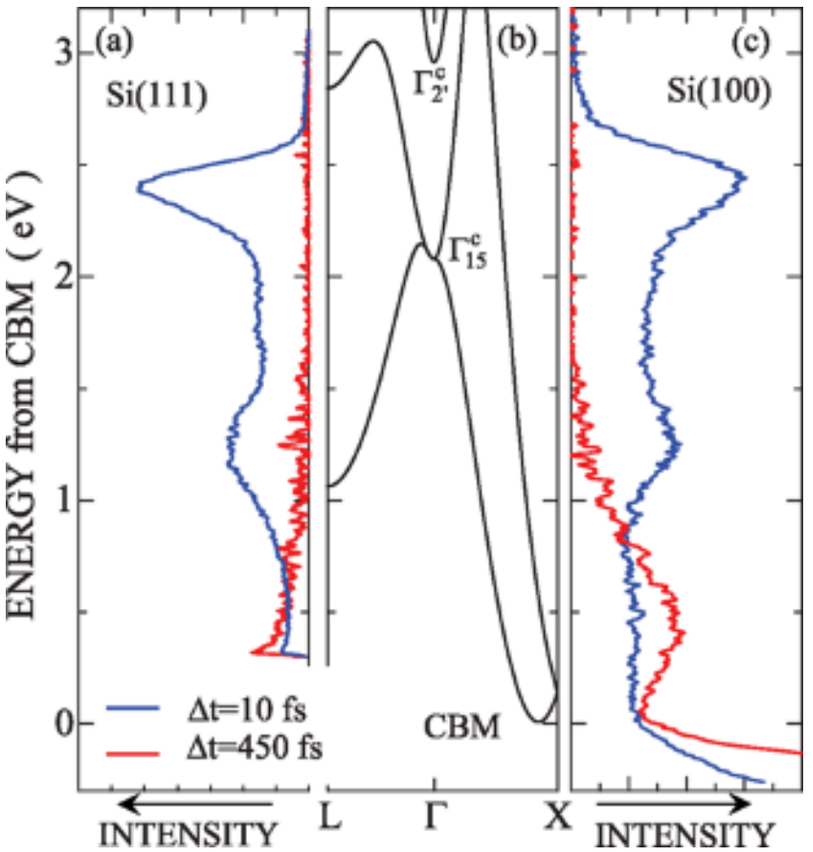

FIG. 2. Silicon at 300 K. (a) Normal photoemission spectra probed by a p-polarised 4.67-eV light at Δt = 10 fs, blue, and at 450 fs, red, for Si(111)- (7 × 7) excited with a s-polarised 3.59-eV light. (b) Conduction-band structure of Si along the $L - \Gamma - X$ directions. Energy is referenced to the conduction band minimum (CBM) thus the scale is that of the excess energy. (c) Normal photoemission spectra probed by a p-polarised 4.67-eV light at Δt = 10 fs, blue, and at 450 fs, red, for Si(001)-(2 × 1) excited with a s-polarised 3.59- eV light. In (a) and (c), the kinetic energies of photoelectrons are referenced to the CBM. Reproduced with permission from Tanimura et al, Phys. Rev. B 100, 035201 (2019). Copyright 2019 American Physical Society.

of the conduction (valence) band[12,50,87]. For "hot" electron distribution, T_e is larger than T_{ph}, where T_{ph} is the lattice temperature. The thermal equilibrium is reached when $T_e = T_{ph}$ and $E^*_f = E_f$. Multiple theoretical works, especially those considering high carrier concentrations, choose "hot" thermal distributions of carriers as the starting point for the description of carrier relaxation dynamics[13]. Indeed, in cases of high carrier concentrations,

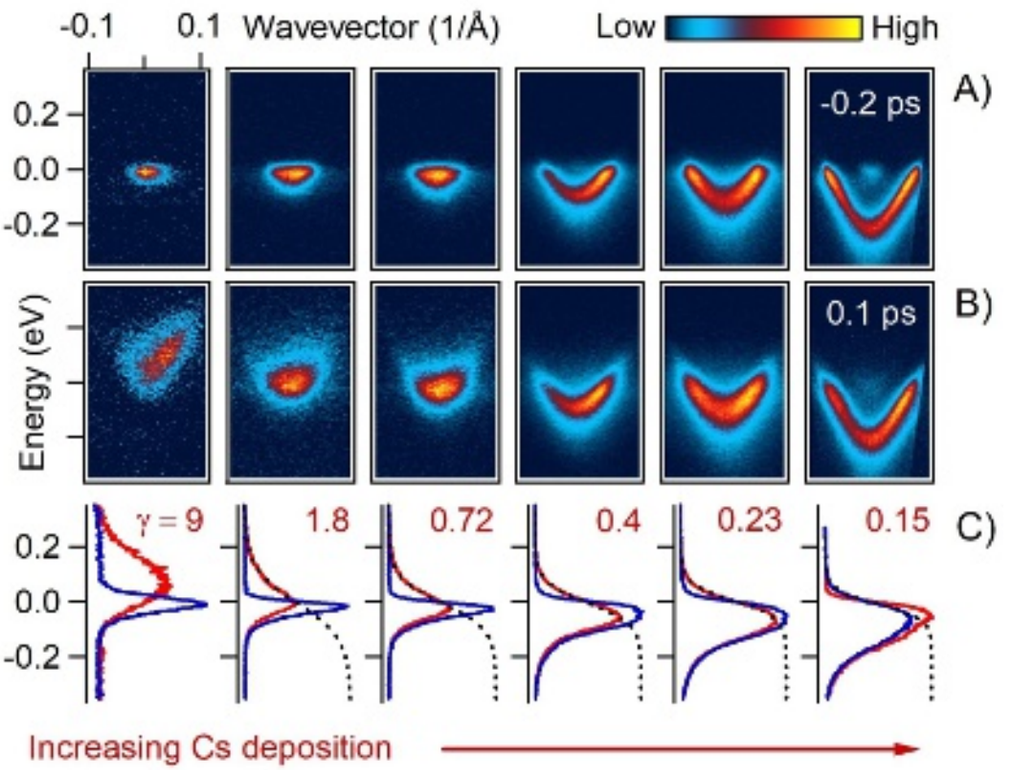

FIG. 3. InSe at 300 K. A) Photoelectron intensity maps acquired at negative pump probe delay. B) Photoelectron intensity maps acquired at delay time of 0.1 ps. C) Wavevector integrated intensity at negative delay time (blue line) and 0.1 ps after photo-excitation (red line). The black dashed line is the estimated Fermi-Dirac distribution. We indicate with γ the ratio between the average excess energy E_x and the Fermi energy E_F. Panels of each column have been acquired for a given exposure to the cesium vapor. From left to right, the Fermi energy of the electron gas is of 10, 40, 65, 95, 130, 180 meV respectively. Adapted from Chen et al, 17, 21962 (2020). Copyright 2020 National Academy of Sciences.

the quasi-thermalization of carriers due to electron-electron interactions is very fast[16,49,57,88]. This is the case in metals[17,61,62,89,90], strongly doped semiconductors[16,91,92], and materials photo-excited with high fluence laser pulses[93].

The interplay between non-thermal and hot electron distributions as a function of carrier concentration is illustrated in Fig. 3, from Ref. 16. In Ref. 16, the relaxation dynamics of photo-excited electrons in InSe was studied as a function of the Cs deposition. The parameter

γ describes the ratio between the average excess energy of photo-excited electrons and the Fermi energy of the electron gas created by Cs deposition. As one can see in Fig. 3, at the lowest Cs deposition ($\gamma = 9$), the photo-excited electron distribution is still non-thermal after a 100 fs delay, whereas at higher deposition levels, the high carrier concentration favors fast thermalization and photo-excited electrons are thermalized in less than 100 fs due to electron-electron interactions.

To conclude, for both non-thermal and quasi-thermalized distributions, the *energy* relaxation of the out-of-equilibrium carriers is usually being discussed. While carrier concentration can be considered as the main parameter governing the formation of quasi-thermalized distributions via electron-electron interactions, the cooling of hot distributions occurs mostly via electron-phonon scattering. Therefore, depending on experimental conditions such as metallicity, doping and laser fluence, the quasi-thermalization due to electron-electron interactions can occur either faster or slower than the energy transfer from electrons to phonons. The main factors governing the strength of the electron-phonon interaction will be discussed in Section III.

B. Momentum distributions

The above-described energy view of carrier distributions leaves out another process, which also occurs at early stages after photo-excitation: the equilibration of carriers in the *momentum* space, leading to the equipartition of the carrier population in the momentum phase space available at a given energy.

Indeed, at early stages after photo-excitation, carriers may populate only part of the available momentum space (see the lower panel of Fig. 1). This typically occurs in many-valley semiconductors photo-excited at energies sufficiently high so that multiple valleys can be populated[12,15,18,60,63], as illustrated in Fig. 4, reprinted from Ref. 60, where a photoemission map of electrons, photo-excited into the conduction band of GaAs with 2.30 eV and 2.07 eV s-polarised light pulses, are shown at different time delays. As one can see in Fig. 4 (upper panel), only the Γ valley is initially populated by photo-excitation, and only later is momentum distributed to the L valley (middle panel) via other processes, such as inter-valley electron-phonon scattering.

Another possibility of creating an unbalanced partition of the carrier population in mo-

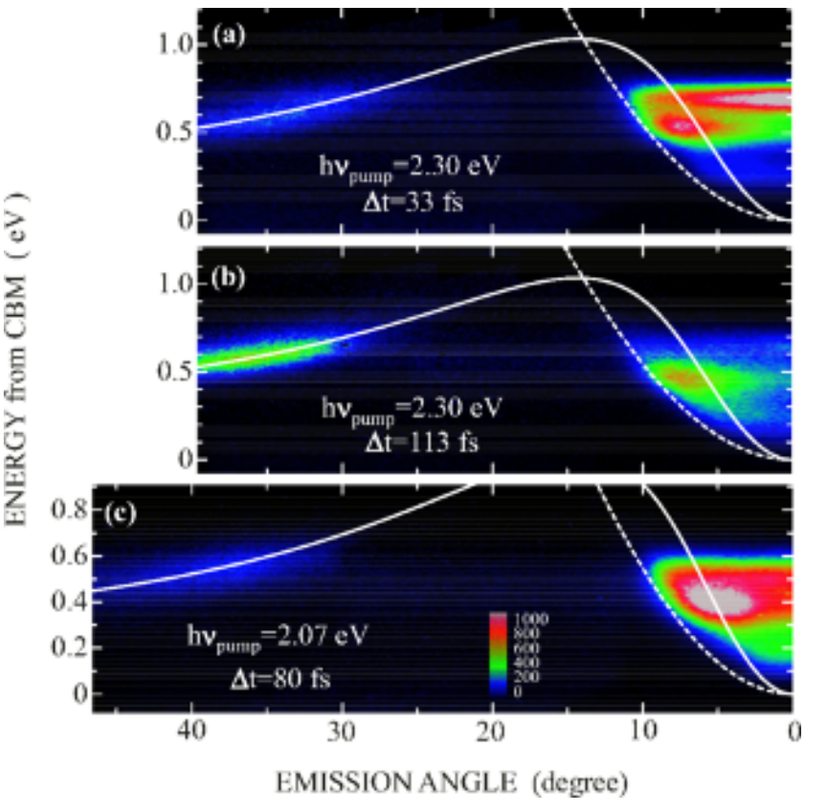

FIG. 4. GaAs at 90 K. (a) The photoemission map for hot electrons injected into the conduction band with *s*-polarised 2.30-eV light pulses, at 33 fs after excitation. (b) The photoemission map for hot electrons injected into the conduction band with *s*-polarised 2.30-eV light pulses, at 113 fs after excitation. (c) The photoemission map for hot electrons injected into the conduction band with *s*-polarised 2.07-eV light pulses, at 80 fs after excitation. The solid and broken curves show the dispersion along Γ-L and Γ-X directions. The color scale indicates the photoemission intensity. Reproduced with permission from Sjakste et al, Phys. Rev. B 97, 064302 (2018). Copyright 2018 American Physical Society.

mentum space, which we call out-of-equilibrium *momentum* space distributions in the following, arises when carriers are photo-excited at the bottom of the conduction band of a many-valley semiconductor using polarised light, which only populates certain valleys, as in the case of dichalcogenides in the context of valleytronics[94–98], as well as in diamond NV centers[99]. Although dichalcogenides and 3D bulk semiconductors such as GaAs or InSe[60,63] are strikingly different materials, the equilibration of carriers in momentum space (between

different valleys) is dominated by the same scattering process: Electron-phonon scattering involving short-wavelength (intervalley) phonons[60,63,96–98]. Depending on materials and experimental conditions, intervalley scattering can occur on very different timescales, ranging from several picoseconds to few femtoseconds. As will be discussed in the next section, in 3D materials such as GaAs or Si, this timescale is mainly determined by the density of the available final states, ranging from picoseconds in the case of scattering between valleys at the bottom of the conduction band[100,101], to a few femtoseconds in the case of highly photo-excited carriers in the upper valleys[18]. However, other factors, such as symmetry selection rules and spin polarisation, also influence significantly the typical scattering timescales in some materials, as in the case of scattering between valley-polarised excitonic states in dichalcogenides[97,98], where electron-phonon scattering timescales are found to be of the order of several picoseconds.

Apart from populating only certain valleys in multivalley materials, photo-excitation with polarised light can lead to the creation of out-of-equilibrium momentum distributions within the same valley[50,102–104]. Such population asymmetry along certain directions in the Brillouin Zone (BZ), caused by the optical selection rules during the photo-excitation, was observed in 3D bulk materials such as GaAs or InP[50,102], in graphene[103], as well as in topological surface states of topological insulators such as Sb_2Te_3[104,105], as one can see in Fig. 5, reprinted from Ref. 104, where the angle-resolved two-photon photoemission (2PPE) data for Sb_2Te_3 photo-excited with mid-IR light are shown. For mid-IR light photo-excitation, the population asymmetry can be clearly seen to last over several hundreds of fs and even at 1 ps delay. In contrast to topological surface states, which typically exhibit much slower intraband dynamics[104,106], in topologically trivial materials such as GaAs and InP, the electrons were found to quasi-equilibrate in momentum space (i.e. lose the initial population asymmetry) within the same valley during the first few tens of fs after photo-excitation, mostly *via* elastic electron-electron scattering[50,102].

As already discussed above for energy distributions, the theoretical methods based on DFT and beyond[66–70,72,73,107] allow the calculation of the out-of-equilibrium initial distributions created by laser pulse in energy and momentum space. However, due to the computational complexity of such methods, the theoretical works focused on the carrier relaxation dynamics at fs and ps scale often use model distributions as a starting point. The out-of-equilibrium character of the initial distributions is mimicked by distributions which occupy

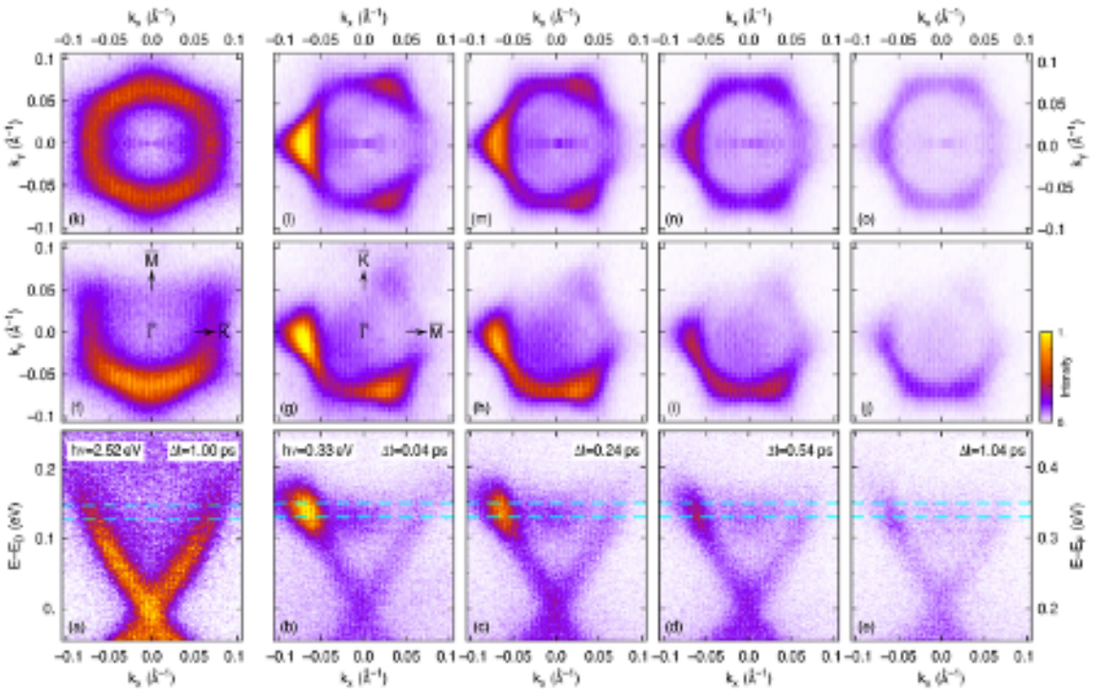

FIG. 5. Sb_2Te_3. Angle-resolved 2PPE data of Sb_2Te_3 excited by visible ($h\nu$= 2.52 eV) and mid-IR ($h\nu$ = 0.33 eV) pump pulses. (a) E–k_x map for 2.52-eV excitation and k_x along $\Gamma - K$ at a pump-probe delay of Δt = 1 ps. (b–e) For 0.33-eV excitation and k_x along $W - K$ at different pump-probe delays as indicated. (f–j) Corresponding k_x–k_y maps integrated over energy intervals depicted by the cyan dashed lines in (a-e). (k-o) The same cuts as (f-j) but with the intensity corrected for the matrix element of the probe transition and symmetrized by mirroring the data at the k_x axis. For all data, the plane of light incidence is oriented along the k_y axis. Reproduced from Reimann et al, Scientific Reports 13, 5796 (2023); licensed under a Creative Commons Attribution (CC BY) license.

only a part of BZ, based on the selection rules for optical transitions, or on the experimental data.[18,40,108]

In summary, the quasi-equilibration of carriers in momentum space for a given energy may be (in limiting cases) faster than, slower than, or on a timescale comparable to the thermalization. The dominant timescale depends on carrier excitation energy, carrier density, and symmetry selection rules. The timescales can range from fs to a few ps, leading to situations in which carriers can be described by different distributions, i.e. out-of-

equilibrium in momentum space and non-thermal[40]; out-of-equilibrium in momentum space but locally quasi-thermalized[12,108]; equilibrated in momentum space but highly non-thermal (hot-electron ensembles discussed below in this work)[15,18]; and finally, equilibrated in momentum space with quasi-thermalized "hot" distributions.[17,61,62] An understanding of which of these regimes is prevalent given the experimental conditions is crucial for the choice of the initial distribution functions.

III. ELECTRON-PHONON SCATTERING OF CARRIERS

A. General framework

As explained in the previous section, electron-phonon scattering determines to a large extent the equilibration of the photo-excited carrier distributions in momentum space, and is also responsible for the transfer of energy from photo-excited electrons to phonons, which takes place for both non-thermal and hot carrier distributions.

When an electron (hole) is photo-excited into the conduction band (valence band) of a semiconductor, its initial position in the BZ is lost rapidly due to both emission and absorption of finite-$\mathbf{q}$ phonons. This loss of the initial momentum can be described by the total electron-phonon scattering rate, or electron-phonon self-energy, which was defined in numerous works[60,61,109,110]. For every initial electronic state $|n,\mathbf{k}\rangle$, the total probabilities for phonon emission and absorption Γ^{em} and Γ^{abs} can be calculated using Fermi's Golden Rule, taking into account all processes allowed by energy and momentum conservation:

$$\begin{aligned}\Gamma_{em} &= \frac{2\pi}{\hbar}\sum_{m\nu}\int\frac{d\mathbf{q}}{\Omega_{BZ}}|g_{mn\nu}(\mathbf{k},\mathbf{q})|^2(N_{\mathbf{q},\nu}+1-f_{m,\mathbf{k}+\mathbf{q}})\delta(\varepsilon_{n,\mathbf{k}}-\varepsilon_{m,\mathbf{k}+\mathbf{q}}-\hbar\omega_{\mathbf{q}\nu})\\ \Gamma_{abs} &= \frac{2\pi}{\hbar}\sum_{m\nu}\int\frac{d\mathbf{q}}{\Omega_{BZ}}|g_{mn\nu}(\mathbf{k},\mathbf{q})|^2(N_{\mathbf{q},\nu}+f_{m,\mathbf{k}+\mathbf{q}})\delta(\varepsilon_{n,\mathbf{k}}-\varepsilon_{m,\mathbf{k}+\mathbf{q}}+\hbar\omega_{\mathbf{q}\nu})\end{aligned} \tag{2}$$

Here, $g_{mn\nu}(\mathbf{k},\mathbf{q})$ is the electron-phonon matrix element, which depends on the initial electronic state $|n,\mathbf{k}\rangle$ with band number n and wavevectror $\mathbf{k}$, on the phonon $|\nu,\mathbf{q}\rangle$, where ν is phonon mode number and $\mathbf{q}$ phonon wave vector, and on the final electronic state $|m,\mathbf{k}+\mathbf{q}\rangle$. The Dirac delta functions $\delta(\varepsilon_{n,\mathbf{k}}-\varepsilon_{m,\mathbf{k}+\mathbf{q}}-\hbar\omega_{\mathbf{q}\nu})$ and $\delta(\varepsilon_{n,\mathbf{k}}-\varepsilon_{m,\mathbf{k}+\mathbf{q}}+\hbar\omega_{\mathbf{q}\nu})$ represent the energy conservation laws for respectively phonon emission and absorption. $f_{n,\mathbf{k}}$ is the carrier distribution function. The possible choices of carrier distributions were discussed above in Section II. The total probability of the electron-phonon scattering for an

electronic state $|n, \mathbf{k}\rangle$ is given by the sum of the emission and absorption probabilities of Eq. 2:

$$\Gamma_{n\mathbf{k}} = \Gamma^{em}_{n\mathbf{k}} + \Gamma^{abs}_{n\mathbf{k}} \tag{3}$$

This total probability describes the loss, by an excited electron, of its initial position in the BZ, i.e. the probability that the $\mathbf{k}$ vector of the initial electronic state will be modified.

The inverse of the total probability of electron-phonon scattering of Eq. 3 yields the "momentum equilibration" time of the electron in a given initial state $|n, \mathbf{k}\rangle$:

$$\tau^{n,\mathbf{k}}_{M} = \frac{1}{\Gamma_{n,\mathbf{k}}}. \tag{4}$$

The rate of the energy transfer from carriers to phonons, reads[60,61,111,112]:

$$\begin{aligned} \frac{\delta E}{\delta t} = \Gamma_{em}\omega_{em} - \Gamma_{abs}\omega_{abs} = \\ 2\pi \sum_{m\nu} \int \frac{d\mathbf{q}}{\Omega_{BZ}} \omega_{\mathbf{q}\nu} |g_{mn\nu}(\mathbf{k}, \mathbf{q})|^2 (N_{\mathbf{q},\nu} + 1 - f_{m,\mathbf{k}+\mathbf{q}}) \delta(\varepsilon_{n,\mathbf{k}} - \varepsilon_{m,\mathbf{k}+\mathbf{q}} - \hbar\omega_{\mathbf{q}\nu}) - \\ -2\pi \sum_{m\nu} \int \frac{d\mathbf{q}}{\Omega_{BZ}} \omega_{\mathbf{q}\nu} |g_{mn\nu}(\mathbf{k}, \mathbf{q})|^2 (N_{\mathbf{q},\nu} + f_{m,\mathbf{k}+\mathbf{q}}) \delta(\varepsilon_{n,\mathbf{k}} - \varepsilon_{m,\mathbf{k}+\mathbf{q}} + \hbar\omega_{\mathbf{q}\nu}) \end{aligned} \tag{5}$$

The strength of the electron-phonon coupling (electron-phonon matrix elements) varies not only for different materials and different scattering channels, but also for every individual transition due to the $\mathbf{k}$- and $\mathbf{q}$-dependences of the matrix elements, which can sometimes be very strong[113], mainly due to symmetry selection rules[114]. Nevertheless, for highly excited carriers, the order of magnitude of the total electron-phonon scattering rate is largely determined by the density of final electronic states (FDOS) available for electron-phonon transitions, as was demonstrated in several previous works[33,36,60,65,115]. This is the reason why the excess energy of carriers, i.e. energy with respect to the bottom of CB (top of the VB) is an important parameter which largely determines the strength of the electron-phonon coupling. The density of final electronic states $FDOS$ represents the phase space available for electron-phonon scattering from a given initial electronic state, and is determined by the energy and momentum conservation rules and by the lattice temperature *via* the phonon occupation numbers (i.e. *via* Bose-Einstein coefficients):

$$FDOS_{n,\mathbf{k}} = \frac{2\pi}{\hbar} \sum_{m\nu} \int \frac{d\mathbf{q}}{\Omega_{BZ}} \left[(N_{\mathbf{q},\nu} + 1) \delta(\varepsilon_{n,\mathbf{k}} - \varepsilon_{m,\mathbf{k}+\mathbf{q}} - \hbar\omega_{\mathbf{q}\nu}) + N_{\mathbf{q},\nu} \delta(\varepsilon_{n,\mathbf{k}} - \varepsilon_{m,\mathbf{k}+\mathbf{q}} + \hbar\omega_{\mathbf{q}\nu}) \right] \tag{6}$$

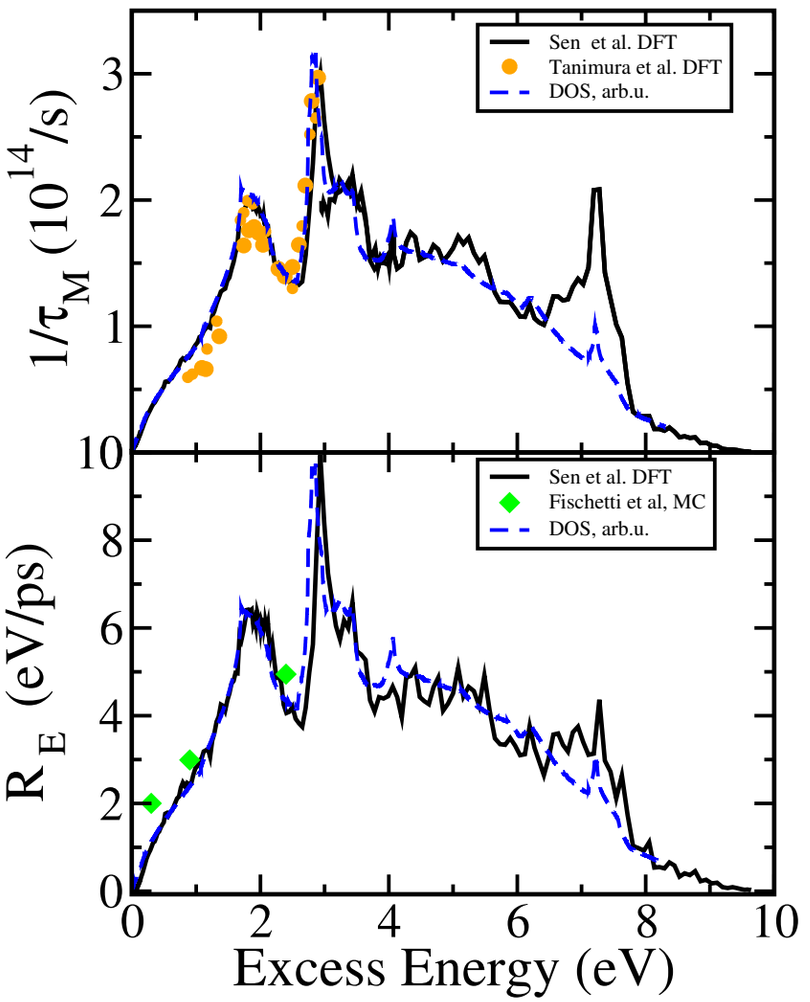

FIG. 6. Silicon at 300 K. Upper panel: total probability of the electron-phonon scattering (Eq. 4), calculated with DFT-based methods for electrons in the lowest conduction band of Si. Black line: Calculated in Ref. 116. Orange circles: From Ref. 18. Lower panel: energy transfer rate from electrons to phonons (Eq. 5). Black line: Calculated in Ref. 116. Green diamonds: From Ref. 117. Blue dashed line: Density of states of the conduction band of silicon, calculated within DFT (arbitrary units). Adapted from Sen et al, Appl. Phys. Lett. 120, 082101 (2022), with the permission of AIP Publishing.

Indeed, in Fig. 6, adapted from Ref. 116, are shown by black lines the total probability of the electron-phonon scattering (Eq. 4) for electrons in the lowest conduction band of Si, calculated at 300 K (upper panel), and the energy transfer rate from electrons to phonons (Eq. 5) (lower panel). As can be seen in Fig. 6, both the total probability of the electron-

phonon scattering and the energy transfer rate follow closely the shape of the density of states (DOS) of the conduction band of Si (blue dashed line).

As one can see in Fig. 6, for silicon at 300 K, at the excess energies above 1 eV, the total probability of electron-phonon scattering corresponds to a momentum equilibration time of less than 10 fs, due to the large densities of final states available for electron-phonon transitions. As discussed in detail in Ref. 2, the momentum equilibration times due to electron-phonon scattering of hot electrons in semiconductors typically range from a few picoseconds at the bottom of the conduction band[55,100,101,118] to a few femtoseconds for high excess energy values[18,65].

B. Electron-phonon scattering rates calculated with DFT-based methods

Methods based on density functional perturbation theory[119,120] for the computation of the electron-phonon coupling matrix elements in metals exist since the late nineties[121,122], and were applied with success for the calculation of the superconducting properties of many materials[123–127]. Calculations of electron-phonon coupling matrix elements in semiconductors appeared somewhat later[128,129]. Today, the *ab initio* calculations of the electron-phonon scattering times and rates in semiconductors, based on the density functional perturbation theory (DFPT)[119,120,130], are performed for calculations of electronic transport[8,131–135], hot electron relaxation[2,15,36,65,136–138], band structure renormalization[139–144], optical absorption[145,146], heat transport[147], exciton-phonon coupling[98,148–150], in bulk 3D materials[33], nanostructures[151–153], alloys[131,154], 2D semiconductors[155–157], perovskites[149,158], and other materials. The possibility to calculate electron-phonon matrix elements and scattering rates with DFT-based methods is provided by numerous widely-used codes, such as Quantum Espresso[159], Abinit[160], VASP[161], EPW[4], Perturbo[162], EPIq[115], to cite but a few. A detailed presentation of the method of calculation of electron-phonon coupling matrix elements based on the density functional perturbation theory (DFPT), as well as a review of applications can be found in Ref. 1. Here, we only briefly mention some general facts and recent advances.

In general, the electron-phonon matrix element is only weakly modified by the type of exchange-correlation functional (for example LDA vs. GGA functionals). Furthermore, *ab initio* calculations of electron-phonon matrix elements beyond the DFT-based description, with methods such as GW, are relatively rare, as they are computationally very expensive. In

the case of diamond, the electron-phonon matrix element at the Γ point was calculated with the GW method in order to study the zero-point renormalization of the band gap[139,143,163,164]. A recent study of several semiconductors[165] concluded that the zero-point renormalization of the band gap of diamond is the only case (among 18 semiconductors considered) were such a description turned out to be really necessary. Also, recently, the projector-augmented-wave (PAW) method for the calculation of the electron-phonon matrix elements has been developed[166,167]. Such a treatment turns out to be important for the electron-phonon matrix elements in cases where the adiabatic approximation reaches its applicability limits[166–168].

In contrast to the electron-phonon matrix element, the choice of the DFT functional can have a strong impact on the calculated band structure, therefore affecting the calculated electron-phonon scattering rates via the density of final electronic states. Although within LDA and GGA, the "scissor shift" approximation can be used to describe the topology of the conduction band[113,129], more elaborate theoretical methods, such as GW for example, are often used in literature nowadays[8,65], to calculate the band structure (eigenenergies of the electronic states), whereas the electron-phonon matrix elements remain calculated on DFT level.

Converged calculations of the integrals such as those of Eq. 3 require a very fine sampling of the **k** and **q** spaces in the BZ, and may therefore involve several hundreds of thousands of electron-phonon matrix elements. Such calculations cannot be carried out directly by DFPT. This issue can be solved by using the interpolation of the electron-phonon matrix elements in the Brillouin Zone, which can considerably reduce the computational load. Interpolation of the electron-phonon matrix elements in the space of maximally localized Wannier functions[169] is one of the most widely used methods of interpolation of the electron-phonon matrix elements[4,110,115,170]. This method, which involves the interpolation of the electron-phonon coupling matrix elements in real space after the transformation to the space of the maximally localized Wannier functions, has been introduced in Refs. 124 and 171. It was then extended to polar materials in Refs. 33 and 172, by adding the analytical description of the Fröhlich interaction using the microscopic model derived by Vogl[173]. More recently, the necessity to also add the quadrupolar interaction[173], even in non-polar materials such as Si, was also demonstrated[34,35]. It must be noted that as an alternative to Wannier functions, in Ref. 174, atomic orbitals bases were proposed for interpolation of the electron-phonon matrix elements. Another possible alternative to Wannier interpolation is a method proposed

more recently, in which the interpolation is performed without using any localised basis sets in real space[34,175]. In the method of Ref. 175, instead of the matrix element, it is proposed to interpolate in real space the lattice-periodic part of the self-consistent perturbing potential induced by the movement of atoms.

It must be also noted that interactions of electrons with two phonons or more phonons, being of the next order in perturbation theory as compared to electron-one-phonon interactions, are generally believed to be negligible. However, it was suggested recently in Ref. 176 that electron-two-phonon interactions for polar optical phonons may play an important role in the description of the mobility in GaAs. Even more recently, the importance of electron-two-phonon interaction for transport simulations in GaAs and in Si was discussed in Refs. 177 and 178. The consensus on the importance of the electron-two-phonon interactions has not yet been reached.

Overall, the predictive capability of the DFT-based calculations of the electron-phonon scattering rates is very good, and was demonstrated by multiple works in the fields of charge transport in 3D and 2D materials[4,8,110,131–133,156,170,178–182], heat transport[147,183], Raman spectroscopy[184–186], coupled charge and heat transport[5,147,187,188], optical spectroscopy[145,146,189], time and angle resolved photoemission spectroscopy (TR-ARPES)[15,16,18,63], superconductivity[121,123–127,190,191] and many others.

Ongoing developments and open questions concern materials with strong anharmonicity[192,193], strong non-adiabaticity[166–168,194–196], exciton-phonon coupling[149,150], polaron coupling[158,197,198], real-space effects[199], the role of screening in 3D and 2D materials[200–202], spin-phonon coupling[203–205], the electron-phonon coupling in correlated materials[162,206], and studies of non-trivial quantum geometry contributions to the electron-phonon coupling[207].

It must be also noted that although DFT-based methods provide access to **k**- and **q**-resolved electron-phonon matrix elements for any transition, the interest for efficient and reliable methods to calculate *effective* electron-phonon matrix elements[208–211] with limited computational effort has been recently renewed, due to 1) increasing complexity (and therefore computational load) of the materials and systems being treated and 2) the necessity to couple DFT-based electron-phonon matrix element with time-dependent transport equations, which will be discussed below.

IV. TIME-DEPENDENT BOLTZMANN EQUATIONS FOR ELECTRONS AND PHONONS

A. General framework

The evolution in time of the out-of-equilibrium carrier distributions can be described by the time-dependent semi-classical Boltzmann equation (t-BTE)[13,212,213]:

$$\frac{\delta f_{\mathbf{k}n}(t)}{\delta t} = \left.\frac{\partial f_{\mathbf{k}n}}{\partial t}\right|_{\text{coll}} \tag{7}$$

Here, we did not consider any external electric or magnetic fields, or temperature gradient[187,212], which would supply additional terms to the carrier BTE. In the absence of such terms, the evolution in time of carrier distributions is determined by the collision term $\left.\frac{\partial f_{\mathbf{k}n}}{\partial t}\right|_{\text{coll}}$, which includes carrier-carrier, carrier-phonon, carrier-impurity contributions.

Full expression of the electron-phonon collision term for charge carriers reads[61]:

$$\begin{aligned}\left.\frac{\partial f_{\mathbf{k}n}}{\partial t}\right|_{\text{coll}}^{\text{e-ph}} = -\frac{2\pi}{\hbar}\frac{1}{\Omega^{BZ}}\sum_{\mathbf{q}m,\nu}|g_{mn\nu}(\mathbf{k},\mathbf{k}')|^2\{&f_{\mathbf{k}n}(1-f_{\mathbf{k}'m})N_{\mathbf{q}}^{\nu}\times\delta(\varepsilon_{\mathbf{k}n}+\hbar\omega_{\mathbf{q}\nu}-\varepsilon_{\mathbf{k}'m})+\\ &f_{\mathbf{k}n}(1-f_{\mathbf{k}'m})(1+N_{\mathbf{q}}^{\nu})\times\delta(\varepsilon_{\mathbf{k}n}-\hbar\omega_{\mathbf{q}\nu}-\varepsilon_{\mathbf{k}'m})-\\ &(1-f_{\mathbf{k}n})f_{\mathbf{k}'m}(1+N_{\mathbf{q}}^{\nu})\times\delta(\varepsilon_{\mathbf{k}n}+\hbar\omega_{\mathbf{q}\nu}-\varepsilon_{\mathbf{k}'m})-\\ &-(1-f_{\mathbf{k}n})f_{\mathbf{k}'m}N_{\mathbf{q}}^{\nu}\times\delta(\varepsilon_{\mathbf{k}n}-\hbar\omega_{\mathbf{q}\nu}-\varepsilon_{\mathbf{k}'m})\}\,.\end{aligned} \tag{8}$$

Here, the final state momentum is denoted $\mathbf{k}' = \mathbf{k} + \mathbf{q}$ to compact the equation.

Similarly to charge carriers, time-dependent BTE can be written for phonons:

$$\frac{\delta N_{\mathbf{q}\nu}(t)}{\delta t} = \left.\frac{\partial N_{\mathbf{q}\nu}}{\partial t}\right|_{\text{coll}} \tag{9}$$

In the case of thermal transport by phonons, phonon-phonon collisions represent the main scattering process at room temperature[214–220], followed by isotope impurity scattering[221–227]. Nevertheless, phonon scattering by electrons (phonon-electron scattering) was also shown to play an important role in heat transport by phonons, especially in doped semiconductors[147,183,228–230].

Importantly, the electron-phonon and phonon-electron terms, which are both due to electron-phonon interaction, couple the carrier and heat transport equations, leading to phenomena such as phonon drag[5,187,188,228,231–233], as well as to dynamical effects due to coupled relaxation dynamics of electrons and phonons[234], such as hot phonon effect[195,235–239], creation

of hot spots in real space[234,240–242], excitation of coherent phonon modes[243–252], time-resolved dynamics of Raman modes[253–255], and photo-excited electron relaxation dynamics[12,14,195].

B. Coupling with *ab initio* data: Scattering mechanisms

The solution of t-BTE for charge carriers requires the description of the electronic band structure, phonon dispersions, and of scattering mechanisms such as electron-electron, electron-phonon, electron-impurity scattering, as well as, eventually, phonon-phonon interactions in cases when coupled electron and phonon dynamics is considered. DFT-based methods which allow to describe various scattering mechanisms can be based on models involving parameters calculated within DFT. For instance, the carrier scattering by charged impurities is often described with the Brooks and Herring model[187,188,256–258]. Additionally, the Fröhlich electron-phonon interaction (polar-optical interaction) can be described using either a macroscopic model[259] or Vogl's microscopic model[33,134,173]. Other electron-phonon scattering channels are often described with effective constants (deformation potentials) as well[99,208,260–263]. The latter treatment of the electron-phonon coupling can, however, lead to the loss of information about the dominating scattering channels[116,264]. Turning to treatment beyond models with DFT-based parameters, an *ab initio* treatment is also possible for carrier scattering by charged impurities.[132,265,266] For the case of electron-phonon scattering, an *ab initio* treatment based on the density functional perturbation theory (DFPT) is widely used[1,119,120,130], as was discussed in detail in section III.

Turning to the scattering mechanisms for t-BTE for phonons, the phonon-phonon scattering, which is the main mechanism limiting phonon lifetimes, can be described via matrix elements for 3-phonon interactions, by the approaches based on the density functional perturbation theory[3,9,215,267], whereas isotope scattering is commonly described by Tamura mass disorder model[268–271]. Further important scattering mechanisms are phonon-electron scattering, which can be described by DFPT as discussed above, and phonon-impurity scattering, which can be described by Tamura model or by approaches beyond Tamura model[272,273].

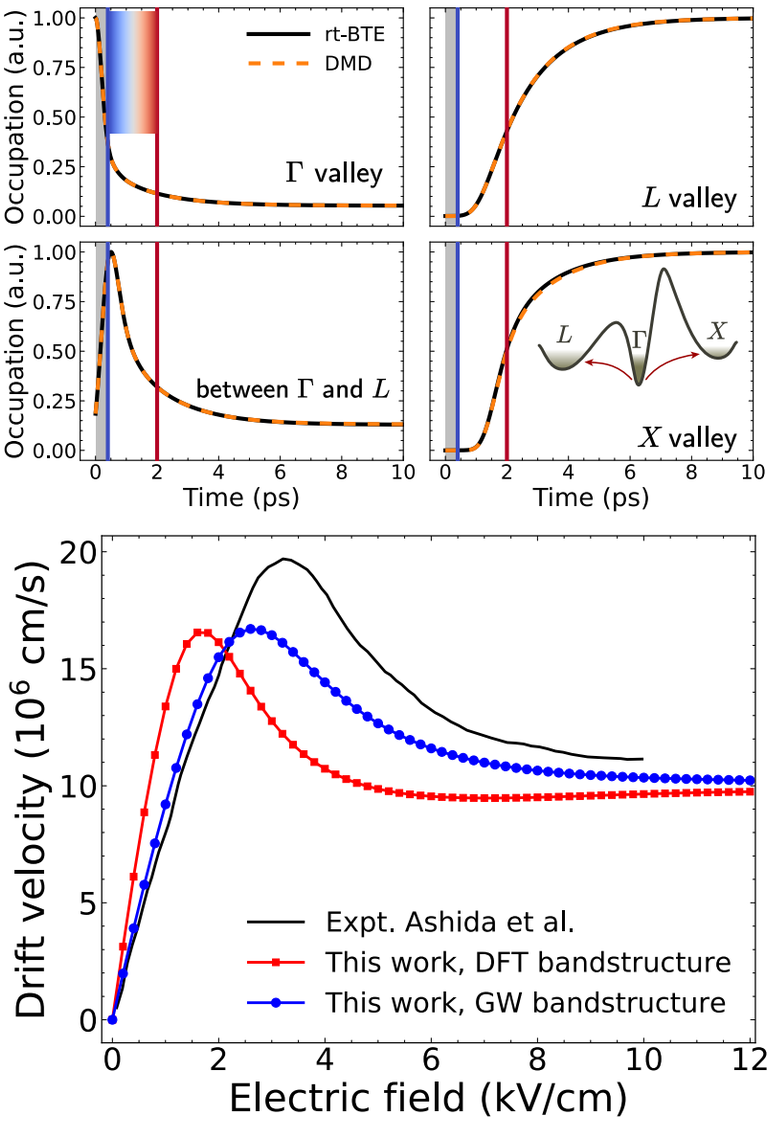

FIG. 7. GaAs at 300K. Upper panel: Time- dependent electron populations of different GaAs valleys, as calculated in Ref. 6 with t-BTE coupled to DFT approach as well as with optimised DMD approach (see text). Reproduced from Maliyov et al, npj Comp. Mat. 10, 123 (2024), licensed under a Creative Commons Attribution (CC BY) license. Lower panel: Velocity-field curve in GaAs at 300 K computed with density functional theory (DFT) and GW band structures in Ref. 7 and compared with experimental data of Ref. 274. In this panel, "This work" refers to Ref. 7. Reproduced with permission from Maliyov et al, Phys. Rev. B 104, L1003303 (2021), Copyright 2021 American Physical Society.

C. Time-dependent BTE solvers coupled with DFT

As discussed in Sec.II, in the most general case of the out-of-equilibrium, non-thermal distributions, the distribution function $f_{\mathbf{k}n}(t)$ of Eq. 7, which depends on the wavevector $\mathbf{k}$ of three (or, eventually, two or one[37,275]) dimensions, on time t and on band index n, is not an analytic function, and should be therefore treated numerically. The implementations of the solution of the t-BTE for out-of-equilibrium, non-thermal distributions are therefore numerically more complex than solutions of the t-BTEs for hot (thermal) carriers. The latter approaches will be discussed in section VI.

The real-time solution of the coupled electron and phonon Boltzmann transport equations, based on explicit time-stepping which allows to follow the changes of the carrier distribution function in real time, applicable to highly out-of-equilibrium, non-thermal distributions, coupled to a completely *ab initio* description of all scattering integrals, was implemented in several recent works, such as for example Refs . 7 and 276. Because of the very high computational cost, first applications of such approaches mostly concerned 2D materials[37], such as graphene[276], which are comparatively more tractable computationally, compared to 3D bulk ones.

For the 3D bulk case, the real-time solution of BTE based on explicit time-stepping with the time step of the order of 1 fs, coupled with fully *ab initio* DFT-based data for band structure, phonons and electron-phonon scattering was implemented recently in Ref. 36 for GaN and in Ref. 7 for GaAs. A subsequent optimisation of this method, based on dynamic mode decomposition (DMD) was recently proposed in Ref. 6. The method allows to follow the out-of-equilibrium carrier populations in time, until they reach a steady state, as one can see on the upper panel of Fig. 7 for GaAs from Ref. 6. In the case shown in Fig. 7, the thermal distribution at 300 K was taken as the initial step, and was evolving in time under applied high electric field. For benchmarking purposes, the numerical application in Refs. 6 and 7 was mainly focused on the transport properties such as velocity-field curve in GaAs, which can be compared with the experimental data (Fig.7, lower panel). Both transient and steady states were studied. Under the applied electric fields considered in Ref. 7, the excess energies of electrons were sufficient to populate the second CB valley (L-valley) of GaAs, and, to some extent, the third valley (X-valley), with the excess energies reaching up to 0.7 eV above the CBM. However, due to very high numerical cost of this method, the highly

non-thermal photo-excited distributions as the ones shown in Fig. 2, with excess energies between 1 and 3 eV above CBM, can hardly be considered, as in that case, the energy and momentum phase space which has to be sampled increases drastically.

In summary, a full-band energy and momentum resolved description of the distribution functions and scattering matrix elements, coupled with time-dependent BTE equations allows the treatment of the most general case of the time evolution of the out-of-equilibrium distribution functions for energy and momentum equilibration taking place on the same timescale[6,7]. This approach is, however, numerically heavy, especially in the case of 3D materials, and can not be easily applied to carriers photo-excited over very large energy intervals. More tractable numerical approaches are possible in cases when momentun equilibration and thermalization occur on different timescales, as we will see in next sections.

V. HOT ELECTRON ENSEMBLE LIMIT

A. HEE concept and its applications

The hot electron ensemble (HEE) idea can be summarized as follows: if the excess energy of photo-excited electrons is sufficiently high, the density of final states available at high excess energies for intervalley electron-phonon scattering is very large, which leads to very fast quasi-equilibration of the electronic distributions in the momentum space (HEE formation), occuring within a few tens of femtoseconds after photo-excitation (or even in few fs): After this initial momentum quasi-equilibration, the electrons can be considered as "spread" over the available phase space in BZ at any given excess energy. The energy transfer from the HEE to the lattice occurs on a much slower timescale, and depends mainly on the excess energy of photo-excited electrons[2,15]. Therefore, HEE idea describes one of the limiting cases in the interplay between energy and momentum equilibration rates, in which momentum equilibration is much faster than the thermalization and cooling (see Fig. 1 and discussion in section II).

The concept of hot electron ensemble (HEE), introduced in Ref. 15, has facilitated the interpretation of a number of time-resolved photoemission experiments[15,16,18,63,277]. It has also facilitated the analysis of the results of other time-resolved spectroscopy methods, such as for example transient absorption spectroscopy results of Ref. 20.

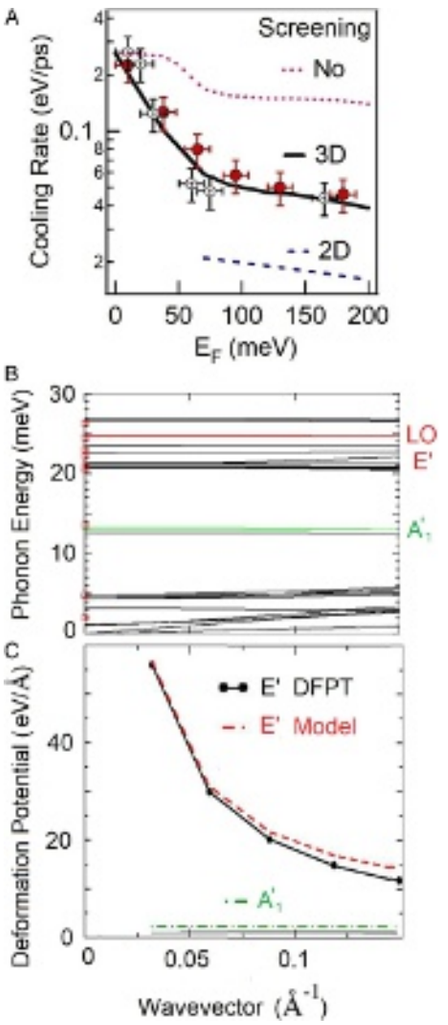

FIG. 8. InSe at 300 K. A) Cooling rate of photo-excited electrons as a function of the Fermi energy of the electron gas created by the Cs deposition (See Fig. 3 and corresponding discussion). Symbols: TR-ARPES measurements. The black solid, blue dashed and red dotted curves are the cooling rates calculated using DFT-based description of the electron-phonon coupling with 3D, 2D and no screening of the Fröhlich interaction, respectively. B) Calculated phonon dispersion of ϵ-InSe in the $\Gamma - M$ direction of the BZ. The polar optical mode E' is shown in red, while the acoustical A'$_1$ mode is shown in green. C) Calculated electron-phonon deformation potentials as a function of the phonon wavevector $\mathbf{q}$ along the $\Gamma - M$ direction. The initial electronic state is in the conduction band at $\mathbf{k} = (0, 0.11, 0)2\pi/a$. For the polar mode, both the results of the DFPT calculation (black circles) and the Vogl model for the Fröhlich coupling (red dotted line) are shown. Reproduced from Chen et al, 17, 21962 (2020). Copyright 2020 National Academy of Sciences.

It must be noted that in some cases the two-photon photoemission experiments were able to capture both the initial momentum quasi-equilibration regime and the energy transfer regime: This was achieved, e.g. in Ref. 15 and 60, for electrons photo-excited in GaAs at excess energies below 1 eV. However, sub-10 fs times which are expected, for example, in the case of electrons photo-excited in Si between 1.1 and 3.2 eV above the CBM[65], are extremely difficult to measure (see Fig. 6 and discussion in Sec. III). Thus, one can expect that for the excess energies which correspond to the momentum equilibration times of the order of a few femtoseconds, only the energy relaxation time scales would be measurable experimentally. This was indeed the case in works such as 16, 18, 63, and 64, where good agreement between energy relaxation times calculated *ab initio* with DFT-based method (Eq. 5), and time-resolved photoemission experiments was achieved, validating the HEE description of photo-excited electron relaxation.

For example, in Ref. 16, the energy transfer from photo-excited electrons to phonons was measured by TR-ARPES in a layered semiconductor InSe, as a function of Cs deposition (see discussion of Fig. 3 in section II), and found to strongly decrease with the increase of Cs deposition, as shown in the upper panel of Fig. 8. In order to explain this experimental result, the energy relaxation rate of Eq. 5 for electrons in InSe was calculated using an *ab initio* description of InSe and the Vogl model[173] for the Fröhlich coupling. To determine the dimensionality of the electron gas, the screening of the Fröhlich coupling was considered in the 3D and 2D cases, using the Thomas-Fermi approach[16,278]. The black line in Fig. 8 shows that the screened 3D Fröhlich interaction better explains the experimentally observed data for the energy transfer rate from photo-excited electrons to phonons.

B. Limitations of the static HEE approach

In Fig. 9, one can see the measured decay times of photo-excited electron population in highly photo-excited silicon, measured by TR-ARPES in Ref. 18 (see Fig. 2 in section II) (symbols). The energy transfer times shown in Fig. 9 by the solid line were obtained from the calculated energy transfer rates of Eq. 5 for Si, which are also shown in Fig. 6 (Sec. III). The energy transfer time from electrons to phonons is defined as the time to transfer the amount of energy ΔE from electrons to phonons[60]. For a given ΔE, the energy transfer

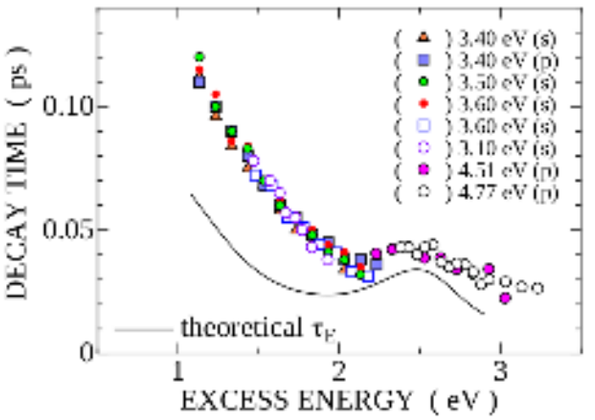

FIG. 9. Silicon at 300 K. Time constant of population decay of hot electrons as a function of the excess energy with respect to the CBM in Si. Symbols represent results obtained by TR-ARPES. Different symbol styles correspond to different pump-photon energies and polarisations. The solid black curve shows the theoretical results of energy transfer time time due to the electron-phonon scattering for ΔE=140 meV, calculated with DFT-based methods. Reproduced with permission from Tanimura et al, Phys. Rev. B 100, 035201 (2019). Copyright 2019 American Physical Society.

time is given by:

$$\tau_E(\varepsilon, \Delta E) = \int_{\varepsilon-\Delta E}^{\varepsilon} d\varepsilon' \frac{1}{\Gamma_{em}\omega_{em}(\varepsilon') - \Gamma_{abs}\omega_{abs}(\varepsilon')} \tag{10}$$

As one can see in Fig. 9, the agreement between theory and experiment is good over the whole range of excess energies considered in Ref. 18, confirming that the measured relaxation rates can be understood as due to energy transfer from electrons to phonons in the framework of the HEE picture.

However, one notes that the calculated energy relaxation times are found to be about 40% shorter than the experimental ones (meaning that the calculated relaxation rates are found to be about 40% higher than the experimental ones). Some of the possible reasons of this discrepancy were discussed and discarded in Ref. 18. Interestingly, our recent results for germanium, shown in Fig. 10, show a similar underestimation between the measured and calculated energy relaxation times.

Indeed, in left panel of Fig. 10, we show the population decay times of hot electrons as a function of the excess energy in Ge, measured using TR-ARPES for ΔE =50 meV at 300 K

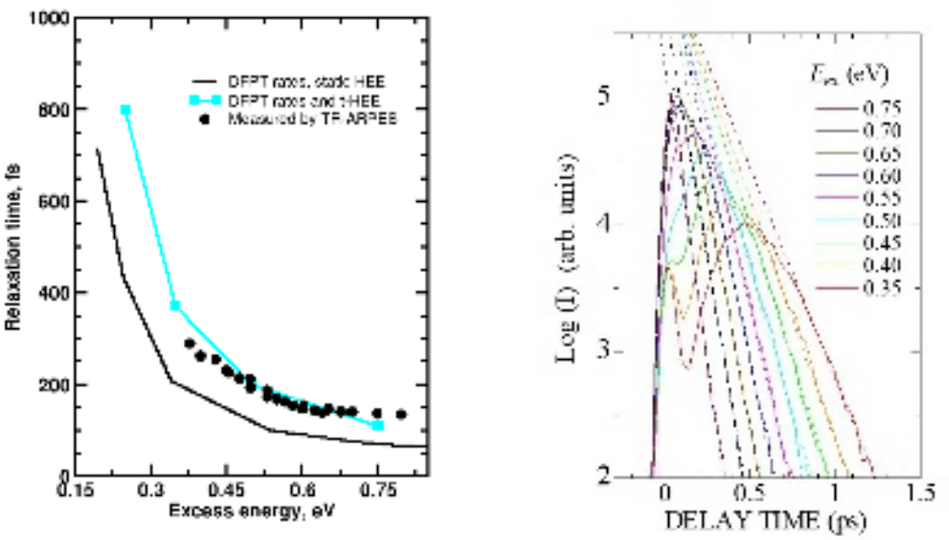

FIG. 10. This work (previously unpublished). Germanium. Left panel: Symbols: The population decay times of hot electrons in Ge, measured by TR-ARPES. Lines: DFT-based calculations of the energy transfer time from electrons to phonons, see text. Right panel: Logarithmic analysis of population intensity, which allows to extract the experimental population decay times.

(symbols). Some experimental details can be found in the note of Ref. 279. In solid line, we show the energy transfer times from electrons to phonons, calculated using Eq. 5 and the DFT-based description of the electron-phonon coupling (see calculation details in Ref. 280). As one can see, similarly to the Si case, the calculated energy transfer times from electrons to phonons were found to be shorter than the experimentally determined ones by about 50%. Here, we propose that the reason for this systematic discrepancy is the evolution of the photo-excited distributions and of the energy transfer rates from electrons to phonons with time. Indeed, in both experiments in Si and Ge, the electronic distributions were photo-excited over large excess energy ranges of several eV, and, for each pulse, the time evolution of the photoemission intensities corresponding to electrons with excess energies from 1 to 2 eV were analysed. In particular, the photoemission intensities, integrated over energy intervals ΔE of 140 meV for Si and of 50 meV for Ge, were analysed at different

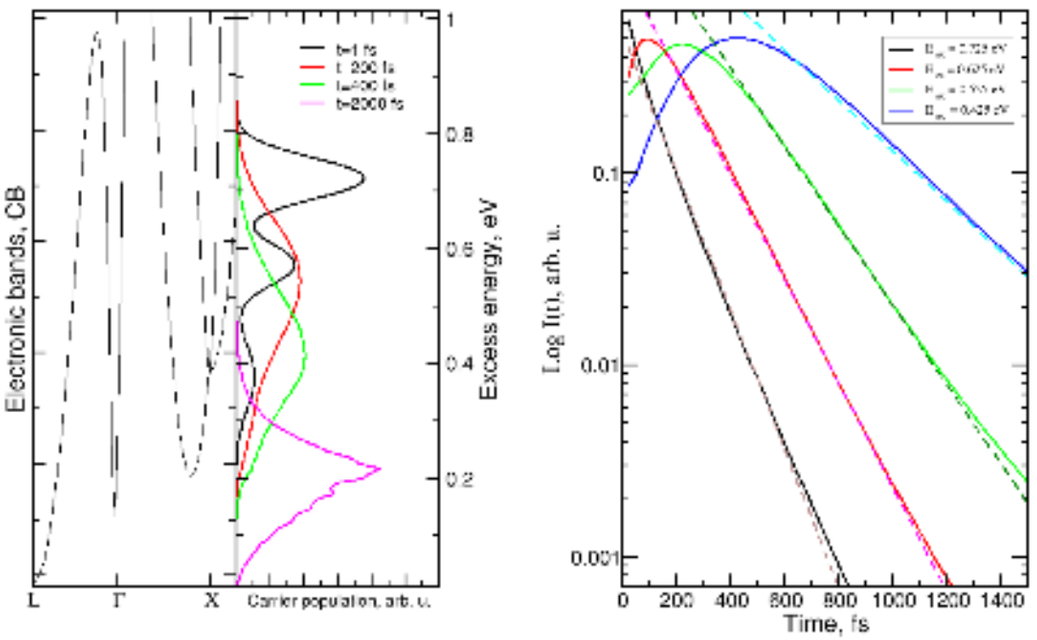

FIG. 11. This work (previously unpublished). Germanium at 300 K. Left panel: Time evolution of photo-excited carrier populations in Ge, described with t-HEE model for Ge (see text). Conduction bands of Ge are shown for guidance. Right panel: Log analysis of calculated integrated carrier populations $I(E_{ex}, \Delta E)$, which allows to extract theoretical decay times.

excess energies for time periods of several hundreds of femtoseconds[18]. The experimental decay rates were then extracted using a semi-logarithmic analysis, as shown in the right panel of Fig. 10 for Ge. However, one can expect the decay rates at a given excess energy to decrease with time, affecting the results of the analysis performed over several hundreds of femtoseconds. Therefore, in order to further improve the agreement between measured and calculated energy transfer times, one needs to describe the evolution of the out-of-equilibrium electronic distributions with time.

C. Time-propagation of the HEE

Here, we present the model of time propagation of the energy-dependent distributions, governed by the energy transfer from electrons to phonons, applicable in the HEE limit. Sim-

ilar ideas of energy-dependent models quasi-equilibrated in momentum space were discussed in other works[62,85,281].

For example, the carrier distribution function averaged over $\mathbf{k}$ space was introduced in Ref. 62:

$$f(\varepsilon) = \frac{1}{n(\varepsilon)} \sum_{\mathbf{k}} \delta(\varepsilon - \varepsilon_{\mathbf{k}}) f_{\mathbf{k}} \tag{11}$$

Here, $n(\varepsilon)$ is the density of states (DOS). Such an approach suggests that very fast quasi-equilibration in momentum space has already taken place, which is in line with the HEE idea for highly photo-excited electrons, as discussed in Sec. II.

The model we are going to present now is very similar to the model of Ref. 62 for nonequilibrium electrons and phonons (NEP) as well as to the approach of Ref. 85, and relies on the fact, discussed above in section III, that the excess-energy dependence of the electron-phonon self-energy, as well as that of the rate of energy transfer from electrons to phonons, follows the excess-energy dependence of the electron density of final electronic states (Fig. 6), as well as on the concept of HEE. The full expression of the electron-phonon collision term, which governs the time evolution of the photo-excited carrier distribution, is given in Eq. 8. In our model, we neglect the wave-vector dependence of all terms, and retain only the excess-energy dependence.

The electron-phonon emission and absorption scattering rates are modeled with the help of the $FDOS$ of Eq. 6, rewritten using effective emission and absorption frequencies ω_{em} and ω_{abs}. Detailed expressions for $FDOS$, emission and absorption scattering rates and the collision term in the framework of this model can be found in the Appendix A.

Then, the time propagation of the electron (or hole) distribution $f(\varepsilon, t)$ can be performed numerically as:

$$f(\varepsilon, t + \Delta t) = f(\varepsilon, t) + \Delta t \left. \frac{\partial f(\varepsilon)}{\partial t} \right|_{\text{coll}}^{\text{e-ph}} (t) \tag{12}$$

As the luminescence intensities are determined by the carrier populations, in Fig. 11 we show an example of the evolution in time of the excess-energy-dependent carrier populations $f(\varepsilon, t)n(\varepsilon)$, where $n(\varepsilon)$ is the electronic DOS of the CB of Ge, calculated with the time-dependent HEE model (t-HEE) for Ge, based on DFT data. The initial distribution was chosen as superposition of three Gaussian functions (black line), in order to mimic the initial photo-excited carrier distribution generated in experiment. From the function shown in the left panel of Fig. 11, one can define a quantity analogous to the experimental integrated

intensity, which was shown in the left panel of Fig. 10), i.e. the carrier population at excess energy E_{ex} integrated over small excess energy interval ΔE:

$$I(E_{ex}, \Delta E) = \int_{E_{ex}-\Delta E}^{E_{ex}} f(\varepsilon, t) n(\varepsilon) d\varepsilon \tag{13}$$

Then, the decay rate of the calculated quantity $I(E_{ex}, \Delta E)$ can be obtained by log analysis, in analogy with the log analysis used to treat experimental data, as shown in Fig. 11, right panel. Finally, as one can see in the left panel of Fig. 10 (cian line), the theory/experiment agreement is improved when the time propagation of HEE is taken into account, explaining the previous discrepancy[18].

More generally, we note that taking into account the realistic out-of-equilibrium electron distribution reduces the energy relaxation rates of highly photoexcited electrons, compared to the case where the calculation is performed with quasi-thermal hot electron distributions, as was previously discussed in Ref. 62. Indeed, in the case of quasi-equilibrated hot distributions, the effect of Pauli blocking factors (see eqns. A2 and A3 in Appendix A) is negligible for electrons belonging to "hot electron tail", as was discussed e.g. in Ref. 16. In contrast, in the case of the out-of-equilibrium electron distributions the Pauli blocking factors may play a significant role at high excess energies, which affects the relaxation dynamics on sub-ps timescales.

VI. TIME PROPAGATION OF QUASI-THERMAL DISTRIBUTIONS

A. Two-temperature model and beyond

The method generally called the two-temperature model (TTM) was first introduced in Refs. 61, 282, and 283 to explain the energy relaxation of hot electrons in metals. As the name of the model implies, it relies on the assumption that electrons and phonons can be described by distinct thermal distributions at any given time. This results from a quasi-thermalization of the distribution of hot electrons in which an electron temperature $T_e > T_{ph}$ is already achieved, as was discussed in section II. The return to equilibrium will then be determined by the rate of energy transfer from electrons to phonons via an expression proportional to the difference between the electron and lattice temperatures, $\frac{\delta E}{\delta t} \propto (T_e - T_{ph})$, which can be obtained from the coupled BTEs of Eqs. 7 and 9 for electrons and phonons[61].

Further approximations such as the Debye approximation for phonons and a single relaxation time approximation for electrons can then be applied to derive an analytical expression for the $\frac{\delta E}{\delta t}$ for metals at low temperature[61,282]. More generally, time-dependent BTE equations for quasi-thermalized hot electron distributions can be solved either analytically or numerically, and have been used to describe the cooling dynamics of photo-excited electons in metals and strongly doped semiconductors[13,284–286].

More recently, the time-dependent coupled BTEs have been combined with a DFPT-based description of all scattering mechanisms for electrons and phonons which can be solved numerically for hot electrons quasi-thermalized in one or several minima of the CB. In this framework, the time-dependent cooling dynamics of hot electrons are described by propagating in time the electronic and lattice temperatures $T_e(t)$ and $T_{ph}(t)$ via coupled equations, as discussed e.g. in Refs. 13 and 287. More broadly, the t-BTEs for quasi-thermalized distributions have been combined with a DFT-based description of all scattering mechanisms in several recent works, such as Refs. 17, 62, and 288 for metals, Refs. 12 and 92 for semiconductors, Refs. 14 and 108 for 2D materials and Ref. 289 and 290 for semimetals. See also the review of Ref. 13 for other examples.

B. Example: Relaxation dynamics of electrons and phonons in Ge

Ref. 12 provides an example of a side-by-side comparison of an x-ray free electron laser (FEL) experiment with from-first-principles DFT/DFPT-based theory including anharmonic phonon scattering that were used to investigate the time-resolved momentum and energy relaxation in photo-excited bulk germanium. The diffuse scattering of femtosecond x-ray pulses allows to directly observe the time-dependence of the phonon distribution in photo-excited Ge[291,292] on picosecond time-scales with femtosecond resolution, as shown in Fig. 12, panels (a)-(c) from Ref. 12 (see also the video in online version of the same reference). In the theoretical model of this work the electron distribution was assumed to be confined to the bottom of several conduction band valleys (index i), and written as a sum of distinct valley contributions, $f^i_{\mathbf{k}}$, each concentrated in one of the conduction band valleys, Γ, L and Δ. It was assumed that fast carrier-carrier scattering establishes a Fermi–Dirac carrier distribution in each valley, with a common temperature T_e for all valleys but a valley-specific chemical potential. Therefore, the study of Ref. 12 represents the case where the carrier

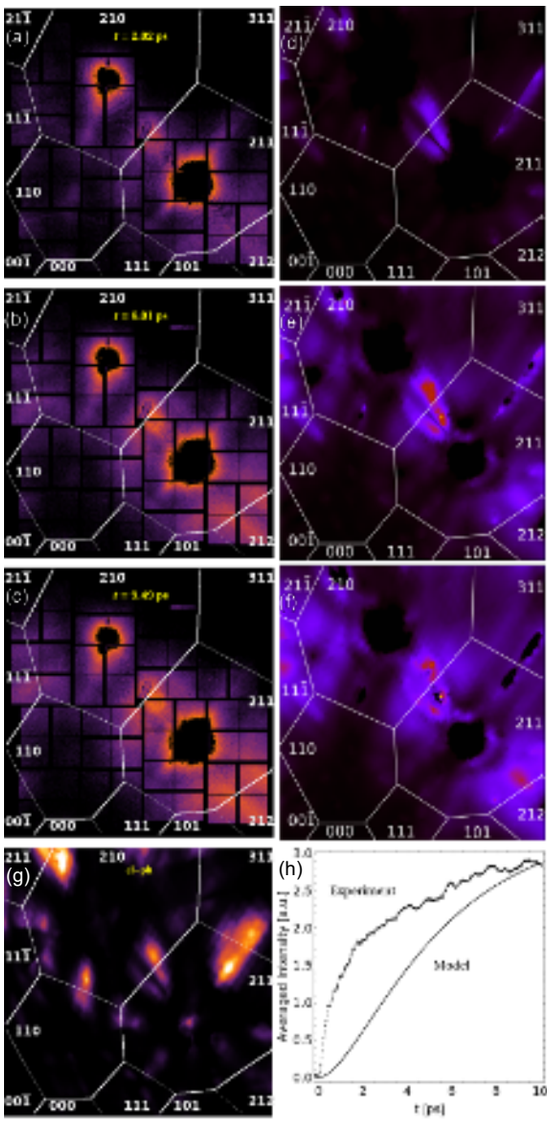

FIG. 12. Ge at 300 K. Top 6 panels: Experimental (a)–(c) and calculated (d)–(f) x-ray intensity at (a) and (d) 2, (b) and (e) 6, and (c) and (f) 9.5 ps after the pump pulse. Points corresponding with the Bragg condition have been removed from (a)–(c) and are ignored in the calculation. Two bottom panels: (g) Intensity due to phonons generated by electron–phonon (el-ph) scattering only, while figures (d)–(f) include el-ph and phonon–phonon scattering. (h) Experimental and calculated x-ray intensity averaged in the region situated at the boundary of zones (210) and (211). Experimental data averaged over 0.33 ps (11 time steps) for smoothness. Reproduced from Murphy-Armando et al, Appl. Phys. Lett. 122, 012202 (2023), with the permission of AIP Publishing.

populations were assumed to be thermalized, but to be out-of-equilibrium in momentum space. A similar study was performed in Ref. 14 for MoS_2. The coupled t-BTEs for electrons and phonons were then solved numerically to describe the evolution of carrier populations in each valley due to intervalley and optical intravalley electron-phonon scattering, and to calculate the transfer of energy and momentum to and from the phonon distribution. A further departure from the TTM is the treatment of a non-thermalized phonon population. The latter was allowed to evolve due to electron-phonon and anharmonic 3-phonon scattering in a 3D grid in momentum space that results in the re-distribution of the energy and momentum of the phonons generated by the relaxation of the electrons via electron-phonon scattering. As can be seen in Fig. 12, the approach of Ref. 12 allows to describe the evolution of non-equilibrium phonon populations on ps scales in agreement with ultra-fast diffuse x-ray scattering FEL experiments. Furthermore, it fully distinguishes features in the diffuse x-ray arising from electron-phonon relaxation or anharmonic 3-phonon decay. For example, the intensity feature at the zone edge in the middle of figures (a)-(f) is due to intervalley electron-phonon scattering between the Δ and L valleys, while the more diffuse intensity 'clouds' around the zone centers are due to anharmonic phonon scattering.

It was shown in 12 that the time-dependent dynamics of phonon distribution significantly impacts the relaxation dynamics of photoexcited electrons. Previously, similar effects of the out-of-equillibrium phonon distribution on the energy transfer from electrons to phonons was discussed in numerous works, e.g. in Ref. 293, where it was shown that taking into account out-of equillibrium phonon distrributions, on ps timescales, leads to decrease of the energy transfrer rate from electrons to phonons.

The work of Ref. 12 also highlights one of the aspects mentioned earlier in section III B regarding the grid density in the calculation of properties that depend on crystal momentum. In many-valley semiconductors, as opposed to metals or highly excited semiconductors[290], the electrons and holes are confined to very small volumes of the BZ. Therefore, the calculation of the phonons generated by the electron-phonon scattering of electrons in these pockets requires a very dense momentum grid for both the phonons and the electrons. In Ref. 12 this was handled with adaptive grids that are dense in the active areas of the BZ, and sparse elsewhere, considerably reducing the computational cost.

VII. PROPAGATION IN TIME USING NON-ADIABATIC MOLECULAR DYNAMICS

A. NAMD: General framework

In previous sections, we have discussed the computational approaches based on coupling of the propagation in time of electronic distributions with the DFPT-based description of the electron-phonon coupling. A DFPT approach does not allow the description of anharmonic effects due to the Born-Oppenheimer approximation used in DFT. Quantum non-adiabatic transitions can not be described because of semi-classical description of carrier dynamics, based on distribution functions and on BTEs. In contrast, the approaches based on non-adiabatic molecular dynamics (NAMD), originally developed in the field of quantum chemistry, which combine the resolution of time-dependent Schrödinger equation and surface hopping, allow to describe both anharmonicity and quantum non-adiabatic transitions[294], by propagating in time the electronic wave function. Originally applied to small molecular systems, such approaches became applicable to extended systems in the classical path approximation, which separates the fast electron dynamics, described by real-time TDDFT, and slow nuclei dynamics, described classically[295,296], while the electron-nuclear interactions are modeled using fewest switching surface hopping[297]. For extended systems, such approaches involve supercells and the reciprocal space is described by the single Γ point or very few $\mathbf{k}$-points, as was done for example in case of perovskites[298], PbSe nanocrystals[299] or topological insulators[300,301]. In this section, we will discuss the first attempts to use the NAMD approach to describe the relaxation dynamics in periodic solids, which have appeared recently[38–40]. In order to achieve this, one has to ensure the description of both zone-center and short-wavelength (intervalley) phonons. The latter can be described either by the use of extremely large supercells, which naturally include all phonons refolded into the Γ point, or by the introduction of the $\mathbf{k}$-dependence of scattering.

B. Example: Photo-excited electron relaxation in Si

In the $\mathbf{k}$-dependent NAMD approach of Ref. 39, the results for the energy relaxation of the photo-excited electron distribution in silicon were found in agreement with the ARPES experiment of Ref. 18, as one can see in Fig. 13 which can be compared to the TR-ARPES

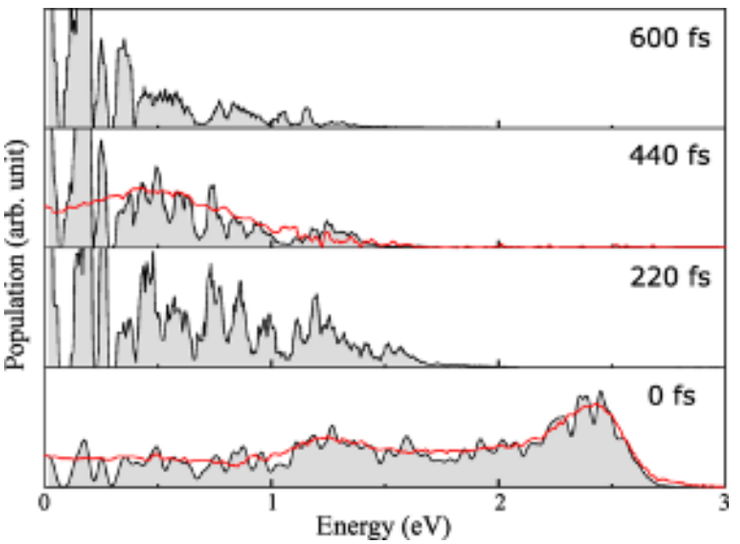

FIG. 13. Silicon. Time evolution of populations of photo-excited electrons in bulk silicon, simulated with the NAMD method in Ref. 39. The red lines are experimentally measured populations from Ref. 18 (Fig. 2). Energy is referred to the conduction band minimum (CBM). Reproduced with permission from Zheng and Wang, Phys. Rev. Lett. 131, 156302 (2024). Copyright 2024 American Physical Society.

results of Fig. 2. Note also that the results of Fig. 13 are similar to the ones obtained for Ge using the time-dependent HEE model (see Fig. 11). As the phonon dispersion was neglected in Ref. 39, the relaxation in momentum space could not be described. One must note however that the result for the energy relaxation was achieved in Ref. 39 by the addition of an effective deformation potential to the nonadiabatic coupling.

This addition of an effective scattering process could be due to the use of relatively sparse **k**-point grids. Indeed, the 4x4x4 **k**-point grids might be insufficient to describe the many-valley band structure of the CB of Si, and therefore underestimate the main electron-phonon scattering process, namely the intervalley scattering between different valleys in Si[18]. One should note that the advantage of the approach of Ref. 39 lies in the natural inclusion of anharmonic effects, crucial for the description of perovskites, graphene and many other anharmonic systems.

Another recent **k**-dependent NAMD-based approach, referred to as NAMD$_k$[38,40], allows to describe the relaxation of carriers in both energy and momentum spaces. In the approach

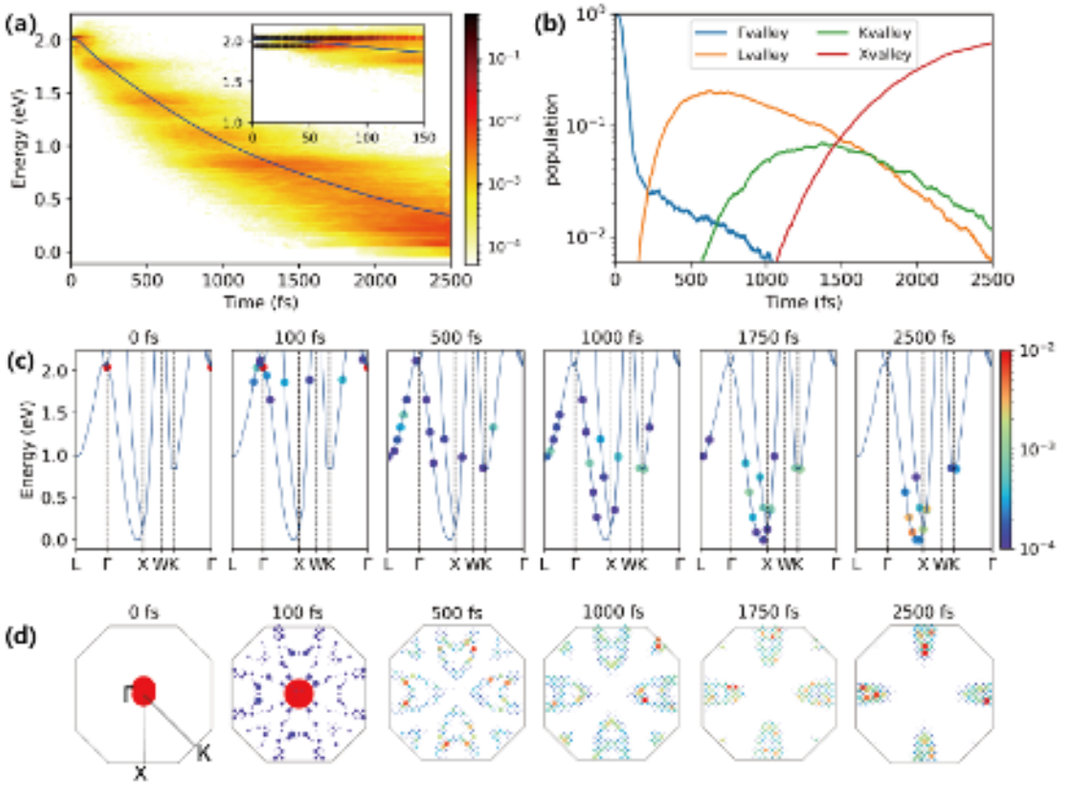

FIG. 14. Silicon. Hot electron relaxation after excitation in the Γ valley of the CB, described with the NAMD$_k$ approach of Refs. 38 and 40. Panel a: Average electron energy vs. time. Panel b: Valley populations. Panel c: Snapshots of the photo-excited electron population in different electronic bands along high symmetric directions in the BZ. Panel d: Snapshots of the photo-excited electron population in the two-dimensional cut of the BZ. Reproduced with permission from Wang et al, J. Phys. Chem. Lett. 15, 3907 (2024). Copyright 2024 American Chemical Society.

of Refs. 38 and 40, the nonadiabatic coupling is replaced with the electron-phonon matrix elements calculated with DFPT, multiplied by time-dependent normal mode coordinate[38]. This allows to achieve the description of the electron-phonon scattering on fine **k**-point grids, and to retrieve the HEE picture of the photo-excited electron relaxation in silicon, as shown in Fig. 14, where one can see both the fast formation of HEE and the slower process of energy transfer from electrons to phonons in Si. The anharmonicity is no longer described due to the use of DFPT, but this does not play any significant role in the case of

Si. One must note, however, that the use of the DFPT description of the electron-phonon matrix elements instead of the nonadiabatic coupling, as well as the stochastic treatment of particle trajectories[40], restricts the applicability of this approach to the weak electron-phonon coupling regime, similarly to other DFPT-based approaches discussed in the present review, such as the DFPT coupled to t-BTEs which was discussed above, or DFPT coupled to Monte Carlo which will be discussed in the next section.

VIII. PROPAGATION IN TIME USING MONTE CARLO METHODS

A. Monte Carlo: General framework

Since the 1970s, the particle Monte Carlo (MC) method for solving the BTE has proven to be a powerful and numerically efficient tool for analysing heat and charge transport in both static and transient regimes in semiconductors[42,56,100,302–309]. These numerical methods stochastically solve the time-dependent BTE, allowing the exploration of transport properties in various physical systems without making assumptions about the shape of the distribution function[261]. This flexibility enables the implementation of all relevant carrier scattering processes already discussed in this review[310–315], as well as spatial carrier scattering, collective plasma effects, and hot phonon effects[316].

MC based aproaches allow to describe transient hot carrier effects[29–32] in both real[234,240–242] and reciprocal spaces. For example, the terahertz response of photo-excited GaAs p-i-n diodes has been studied in Ref. 317 using the MC approach, which allows to capture the evolution of the carrier distributions in both real and reciprocal spaces. The MC approach has also been used for studying avalanche photodiodes, where both the high electric fields and the description of the hot carriers are critical[41,318,319]. Moreover, the MC approach to hot carrier transport has been used to study the ultrafast carrier dynamics in photoconductive samples[320], to interpret experiments on the valley-polarisation of electrons in solids[99], to describe transport properties in thermoelectric materials[42,211], spin relaxation dynamics[321] as well as to describe charge carrier relaxation in semiconductors[322], wide band gap materials[323], 2D materials[324] and quantum wells[325].

B. Coupling with DFT

Initially, semi-classical approaches relied heavily on semi-empirical band structures. These methods used analytical representations of band structures based on the electronic effective masses and parameters describing the non-parabolicity of the electronic bands[261], whereas the scattering rates were determined using an empirical set of deformation potentials[260,261,326–328]. A full-band description of the band structure (i.e. the energies and velocities implemented for states at all **k** points) has also been introduced in MC calculations, with the band structure being described with an empirical framework such as the **k**.**p** method[329] or the empirical pseudopotential approach[318,319,330]. To limit computational costs, a semi-analytical expansion of the energy bands has also been efficiently implemented using spherical harmonic expansions[331]. Finally, DFT has been introduced to describe electronic band structures, allowing for an accurate representation of band structures without the need of prior experimental data[332]. This shift from empirical to from-first-principles approaches marks a significant improvement in the predictive power of transport calculations[332].

Additionally, DFT can be employed to compute deformation potentials directly from first principles in predicting scattering rates and transport properties under various conditions[101,333]. A discussion and additional references can be found e.g. in Ref. 328. Some of the specific problems encountered when the effective electron-phonon coupling constants calculated with DFT-based methods are coupled with MC approaches were discussed recently e.g. in Ref. 116 for silicon, and in Refs. 177 and 334 for GaAs.

Nowadays, the full parametrization of MC methods using both DFT calculations for band structure and the **k**- and **q**-resolved DFPT-based description of the electron-phonon scattering matrix elements, which mark a significant advancement in charge transport modeling, are starting to appear in litterature[323,324,335,336]. It must be noted, however, that due to the necessity to use very fine **k** and **q** grids for the accurate description of scattering rates, this coupling of DFT-based description of scattering and of MC transport simulations encounters, for 3D materials, similar computational problems as the ones discussed above in Sec. IV for DFT coupling with t-BTEs[335]. Overcoming these issues for 3D materials will greatly enhance our understanding of hot carriers in nanoscale semiconductor devices.

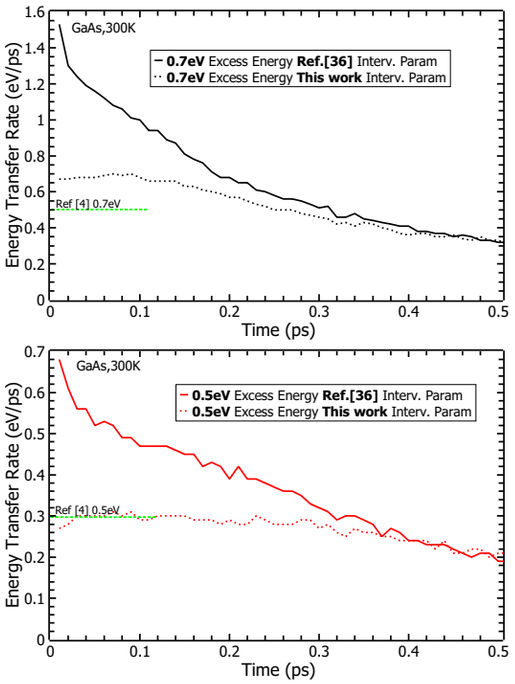

FIG. 15. GaAs at 300 K. MC simulation of the evolution with time of the energy transfer rate from electrons to phonons, for the out-of-equilibrium carrier distributions excited initially at 0.7 eV (upper panel) and 0.5 eV (lower panel) above the CBM. The values of the energy transfer rate from photo-excited electrons to phonons in GaAs, measured in Ref. 60 using time-resolved photoemission are indicated by the green lines. Reproduced from Ghanem et al, Proceedings of SPIE 12992, 1299207 (2024). Copyright 2024 SPIE.

C. Example: Transient transport regime in GaAs

In the present example, we discuss the coupling of the device-oriented stochastic MC approach[41,337,338] with the *ab initio* description of the electron-phonon coupling[33,115], in the case of GaAs, in the recent work of Ref. 43.

This example focused specifically on the energy transfer from electrons to phonons in the transient regime, which is governed by the intervalley electron-phonon scattering, as was shown e.g. in Ref. 60.

In Fig. 15 from Ref. 43, the MC results for transient transport regime in GaAs were obtained with the intervalley scattering constants of Ref. 339 (solid curves) and with the ones determined from the DFT-based description as explained in Ref. 43(dashed curves).

Fig. 15 shows the evolution with time of the energy transfer rate from electrons to phonons, for the out-of-equilibrium carrier distributions excited initially at 0.5 eV and 0.7 eV above the conduction band minimum, which were modeled by Gaussian functions centered around 0.5 eV and 0.7 eV excess energies. As one can see in Fig. 15, at early times, the change in the intervalley scattering constant strength changes strongly the energy transfer rate from electrons to phonons[60]. Interestingly, as one can see in Fig. 15, for time values greater than 0.4 ps, the energy transfer rate is no longer affected by the drastic change in the intervalley scattering parameters. Finally, as shown in Fig. 15, MC results using DFT-based values are found in good agreement with the experimental energy transfer rate from photo-excited electrons to phonons, which was measured in Ref. 60 using time-resolved photoemission.

D. Beyond BTE: Quantum effects

Since the BTE includes the effect of the electrostatic potential only through its first order gradient, the electric field, that acts on the point particles according to classical mechanics, it cannot include any quantum transport effect such as tunneling or quantum reflection related to the coherence of the electron wave function. However, the BTE is nothing else than the semi-classical approximation of the more general Wigner transport equation (WTE) that fully includes the quantum effects induced by the electrostatic environment in which electron wave functions move[340]. It was shown that the Monte Carlo algorithms used to solve the BTE for semi-classical particles can be extended to the solution of the WTE for quantum pseudo-particles[341,342]. For practical numerical simulations, an approximation must be however done for the treatment of electron scattering by phonons or ionized impurities. The approximation consists in considering the weak coupling limit and assuming the duration of the interaction to be much smaller than other phenomena at play, which results in a scattering operator exactly equal to that in the Boltzmann formalism. This simplified approach of scattering neglects advanced quantum effects of electron or phonon coupling like collisional broadening and retardation or intracollisional field effects, but it has been shown to describe very well the phonon-induced decoherence of electrons in nanostructures[343]. Additionally, this so-called Wigner-Boltzmann Monte Carlo approach works remarkably well to describe quantum transport effects in devices like resonant tunneling diodes[344] and nano-transistors[345]. Recent research works in the field are mainly dedicated to more advanced quantum problems like for

instance the simulation of indistinguishable fermions in the many-body Wigner formalism[346], the combination of neural networks and quantum particles to simulate quantum systems efficiently[347], or the investigation of the entanglement of electrons in nanostructures with a single dopant using Wigner-Poisson coupling[348].

IX. CONCLUSION AND PERSPECTIVES

In this work, we have attempted to discuss the relaxation of out-of-equilibrium carriers in the context of several time-resolved spectroscopy experiments, as well as in the context of hot carrier transport. We have shown that the same theoretical approaches can be applicable to describe transient transport and transient spectroscopy, which greatly increases the possibilities to benchmark new computational methods and to confront them to the experimental data and to previous theoretical results.

We have reviewed modern state-of-the-art computational methods, based on the DFT and on the time-dependent solution of Boltzmann transport equations, which allow to describe the return to equilibrium of out-of-equilibrium carrier distributions, in various materials under various types of perturbation. Among the numerous works available in literature on this subject, we have chosen examples mainly focused on 3D semiconducting materials, and on the role of electron-phonon coupling. As we have shown, somewhat surprisingly, the "simple" 3D materials present computational and numerical challenges, inherent to all approaches which couple *ab initio* full-band momentum-resolved scattering rates and time-stepping of transport equations, whether in the case of t-BTEs, Monte Carlo, or non-equilibrium molecular dynamics. This is why the ongoing efforts concern the optimisation of numerical cost and the development of machine-driven optimisation methods[6,191,349–351]. Moreover, recently, deep-learning approaches to DFT[352] and DFPT[353] are starting to be actively developed.

At the same time, by a judicious use of approximations and by limiting the application range, numerous theoretical approaches provide the description of carrier relaxation dynamics at reduced computational cost and without loss of physical insight nor predictive capability, as in cases of HEE or of beyond-TTM approaches. The choice of the method depends on the dominant process that makes the system of electrons and phonons return to equilibrium, which mainly depends on the carrier concentration and on the available density

of final states.

Finally, we mention that, apart from the NAMD and WTE approches we have discussed, which allow to describe anharmonic transitions and quantum effects, numerous other recent theoretical developments open the way to describe time-dependent phenomena related to electron-phonon coupling beyond the scope of this review, such as, for example, decoherence induced by the electron-phonon coupling[354] and many others.

Appendix A

Here, we provide some details on the t-HEE model discussed in section V.

The electron-phonon emission and absorption scattering rates are modeled with the help of the $FDOS$ of Eq. 6, rewritten using effective emission and absorption frequencies ω_{em} and ω_{abs}:

$$FDOS(\varepsilon) = FDOS_{em}(\varepsilon, \omega_{em}) + FDOS_{abs}(\varepsilon, \omega_{abs}) = \frac{2\pi}{\hbar}\Sigma_m \int \frac{d\mathbf{k}}{\Omega_{BZ}} \delta(\varepsilon - \varepsilon_{m,\mathbf{k}} - \hbar\omega_{em})(N(\omega_{em}) + 1) + \frac{2\pi}{\hbar}\Sigma_m \int \frac{d\mathbf{k}}{\Omega_{BZ}} \delta(\varepsilon - \varepsilon_{m,\mathbf{k}} + \hbar\omega_{abs}) N(\omega_{abs}) \tag{A1}$$

Here, $N(\omega)$ is phonon distribution function, which is assumed to be Bose-Einstein equilibrium function at $T = 300$ K in this example, and therefore the heating of phonon modes due to energy transfer from photoexcited electrons is neglected. It is also possible to consider nonthermal phonon distributions, which would imply solving coupled BTEs for electrons and phonons.

Then, the emission and absorption probabilities are approximated as:

$$\begin{aligned} \Gamma_{em}(\varepsilon) &= C_{elph} FDOS_{em}(1 - f(\varepsilon - \hbar\omega_{em})) \\ \Gamma_{abs}(\varepsilon) &= C_{elph} FDOS_{abs}(1 - f(\varepsilon + \hbar\omega_{abs})) \end{aligned} \tag{A2}$$

Here, C_{elph} is a constant adjusted on the DFT-based electron-phonon self-energy.

The collision term becomes:

$$\left.\frac{\partial f(\varepsilon)}{\partial t}\right|_{\text{coll}}^{\text{e-ph}} = -C_{elph}[FDOS_{em} f(\varepsilon)(1 - f(\varepsilon - \hbar\omega_{em})) + FDOS_{abs} f(\varepsilon)(1 - f(\varepsilon + \hbar\omega_{abs})) - FDOS_{em} f(\varepsilon - \hbar\omega_{em})(1 - f(\varepsilon)) - FDOS_{abs} f(\varepsilon + \hbar\omega_{abs})(1 - f(\varepsilon))] \tag{A3}$$

ACKNOWLEDGMENTS

JS, RS, JSM, MG, NV and PD acknowledge financial support from the ANR PLACHO project ANR-21-CE50-0008. FMA acknowledges SFI award 19/FFP/6953 for funding his contribution. JK acknowledges financial support from the JSPS Grants-in-Aid (Grant Number 23540366 and 19H01826). Computer time has been granted by the national centers GENCI-CINES and GENCI-TGCC (Project 2210), and by École Polytechnique through the 3Lab computing cluster.

JS, NV and JK gratefully acknowledge many years of fruitful collaboration with Prof. Katsumi Tanimura.

REFERENCES

[1]F. Giustino, Rev. Mod. Phys. **89**, 015003 (2017), and refererences herein.

[2]J. Sjakste, K. Tanimura, G. Barbarino, L. Perfetti, and N. Vast, J. Phys.: Condens. Matter **30**, 353001 (2018).

[3]L. Paulatto, F. Mauri, and M. Lazzeri, Phys. Rev. B **87**, 214303 (2013).

[4]H. Lee, S. Poncé, K. Bushick, S. Hajinazar, J. Lafuente-Bartolome, J. Leveillee, C. Lian, J.-M. Lihm, F. Macheda, H. Mori, H. Paudyal, W. H. Sio, S. Tiwari, M. Zacharias, X. Zhang, N. Bonini, E. Kioupakis, E. R. Margine, and F. Giustino, npj Computational Materials **9** (2023), 10.1038/s41524-023-01107-3.

[5]R. Sen, N. Vast, and J. Sjakste, Phys. Rev. B **108**, L060301 (2023).

[6]I. Maliyov, J. Yin, J. Yao, C. Yang, and M. Bernardi, npj Comput Mater **10**, 123 (2024).

[7]I. Maliyov, J. Park, and M. Bernardi, Phys. Rev. B **104**, L100303 (2021).

[8]S. Poncé, W. Li, S. Reichardt, and F. Giustino, Rep. Prog. Phys. **83**, 036501 (2020).

[9]L. Paulatto, D. Fournier, M. Marangolo, M. Eddrief, P. Atkinson, and M. Calandra, Phys. Rev. B **101**, 205419 (2020).

[10]G. Fugallo and L. Colombo, Phys. Scr. **93**, 043002 (2018).

[11]A. Cepellotti and N. Marzari, Phys. Rev. X **6**, 041013 (2016).

[12]F. Murphy-Armando, E. D. Murray, I. Savić, M. Trigo, D. A. Reis, and S. Fahy, Appl. Phys. Lett. **122**, 012202 (2023).

[13]F. Caruso and D. Novko, ADVANCES IN PHYSICS: X **7**, 2095925 (2022).

[14]F. Caruso, J. Phys. Chem. Lett. **12**, 1734 (2021).

[15]H. Tanimura, J. Kanasaki, K. Tanimura, J. Sjakste, N. Vast, M. Calandra, and F. Mauri, Phys. Rev. B **93**, 161203(R) (2016).

[16]Z. Chen, J. Sjakste, J. Dong, A. Taleb-Ibrahimi, J.-P. Rueff, A. Shukla, J. Peretti, E. Papalazarou, M. Marino, and L. Perfetti, PNAS **117**, 21962 (2020).

[17]P. Maldonado, K. Carva, M. Flammer, and P. M. Oppeneer, Phys. Rev. B **96**, 174439 (2017).

[18]H. Tanimura, J. Kanasaki, K. Tanimura, J. Sjakste, and N. Vast, Phys. Rev. B **100**, 035201 (2019).

[19]M. Zürch, H.-T. Chang, L. J. Borja, P. M. Kraus, S. K. Cushing, A. Gandman, C. J. Kaplan, M. H. Oh, J. S. Prell, D. Prendergast, C. D. Pemmaraju, D. M. Neumark, and S. R. Leone, Nat. Commun. **8**, 15734 (2017).

[20]M. Wörle, A. W. Holleitner, R. Kienberger, and H. Iglev, Phys. Rev. B **104**, L041201 (2021).

[21]A. L. Cavalieri, N. Müller, T. Uphues, V. S. Yakovlev, A. Baltuška, B. Horvath, B. Schmidt, L. Blümel, R. Holzwarth, S. Hendel, M. Drescher, U. Kleineberg, P. M. Echenique, R. Kienberger, F. Krausz, and U. Heinzmann, Nature **449**, 1029 (2007).

[22]M. Ossiander, J. Riemensberger, S. Neppl, M. Mittermair, M. Schäffer, A. Duensing, M. S. Wagner, R. Heider, M. Wurzer, M. Gerl, M. Schnitzenbaumer, J. V. Barth, F. Libisch, C. Lemell, J. B. ürfer, P. Feulner, and R. Kienberger, Nature **561**, 374 (2018).

[23]T. Hopper, A. Gorodetsky, J. Frost, C. Müller, R. Lovrincic, and A. Bakulin, ACS Energy Lett. **3**, 2199 (2018).

[24]P. P. Joshi, S. F. Maehrlein, and X. Zhu, Advanced Materials **31**, 1803054 (2019), https://onlinelibrary.wiley.com/doi/pdf/10.1002/adma.201803054.

[25]M. Na, A. K. Mills, and D. J. Jones, Physics Reports **1036**, 1 (2023), advancing time- and angle-resolved photoemission spectroscopy: The role of ultrafast laser development.

[26]D. A. Zimin, N. Karpowicz, M. Qasim, M. Weidman, F. Krausz, and V. S. Yakovlev, Nature **618**, 276 (2023).

[27]P. D. Ndione, S. T. Weber, D. O. Gericke, and B. Rethfeld, Scientific Reports **12**, 4693 (2022).

[28]F. Boschini, M. Zonno, and A. Damascelli, Rev. Mod. Phys. **96**, 015003 (2024).

[29]A. J. Nozik, Nature Energy **3**, 170 (2018).

[30]C. Y. Tsai, Solar Energy **188**, 450 (2019).

[31]D. König, Y. Yao, B. Puthen-Veettil, and S. C. Smith, Semiconductor Science and Technology **35**, 073002 (2020).

[32]C. Liu, Y. Lu, R. Shen, Y. Dai, X. Yu, K. Liu, and S. Lin, Nano Energy **95**, 106977 (2022).

[33]J. Sjakste, N. Vast, M. Calandra, and F. Mauri, Phys. Rev. B **92**, 054307 (2015).

[34]G. Brunin, H. P. C. Miranda, M. Giantomassi, M. Royo, M. Stengel, M. J. Verstraete, X. Gonze, G.-M. Rignanese, and G. Hautier, Phys. Rev. Lett. **125**, 136601 (2020).

[35]V. A. Jhalani, J.-J. Zhou, J. Park, C. E. Dreyer, and M. Bernardi, Phys. Rev. Lett. **125**, 136602 (2020).

[36]V. Jhalani, J. Zhou, and M. Bernardi, Nano Lett. **17**, 5012 (2017).

[37]I. Wadgaonkar, M. Wais, and M. Battiato, Computer Physics Communications **271**, 108207 (2022).

[38]Z. Zheng, Y. Shi, J.-J. Zhou, O. V. Prezhdo, Q. Zheng, and J. Zhao, Nat Comput Sci **3**, 532 (2023).

[39]F. Zheng and L.-W. Wang, Phys. Rev. Lett. **131**, 156302 (2023).

[40]Z. Wang, Z. Zheng, Q. Zheng, and J. Zhao, J. Phys. Chem. Lett. **15**, 3907 (2024).

[41]A. Pilotto, M. Antonelli, F. Arfelli, G. Biasiol, G. Cautero, M. Cautero, M. Colja, F. Driussi, D. Esseni, R. H. Menk, C. Nichetti, F. Rosset, L. Selmi, T. Steinhartova, and P. Palestri, Frontiers in Physics **10**, 944206 (2022).

[42]P. Priyadarshi and N. Neophytou, Journal of Applied Physics **133** (2023), 10.1063/5.0134466.

[43]M. Ghanem, P. Dollfus, J. Saint Martin, R. Sen, N. Vast, and J. Sjakste, Proceedings of SPIE - The International Society for Optical Engineering **12992** (2024), 10.1117/12.3022114.

[44]M. Lundstrom, Measurement Science and Technology **13**, 230 (2002).

[45]R. ALFANO, ed., *Semiconductors Probed by Ultrafast Laser Spectroscopy* (Academic Press, 1984).

[46]J. Shah, "Ultrafast spectroscopy of semiconductors and semiconductor nanostructures," (Springer, Berlin, 1999) 2nd ed.

[47]J. Lloyd-Hughes, P. Oppeneer, T. Pereira Dos Santos, A. Schleife, S. Meng, M. Sentef, M. Ruggenthaler, A. Rubio, I. Radu, M. Murnane, X. Shi, H. Kapteyn, B. Stadtmüller,

K. Dani, F. Da Jornada, E. Prinz, M. Aeschlimann, R. Milot, M. Burdanova, J. Boland, T. Cocker, and F. Hegmann, J. Phys.: Condens. Matter **33** (2021), 10.1088/1361-648X/abfe21.

[48]M. Sentef, A. F. Kemper, B. Moritz, J. K. Freericks, Z.-X. Shen, and T. P. Devereaux, Phys. Rev. X **3**, 041033 (2013).

[49]J. Kanasaki, H. Tanimura, K. Tanimura, P. Ries, W. Heckel, K. Biedermann, and T. Fauster, Phys. Rev. B **97**, 035201 (2018).

[50]H. Tanimura, K. Tanimura, and J. Kanasaki, Phys. Rev. B **104** (2021), 10.1103/PhysRevB.104.245201.

[51]M. Lian, Y.-C. Wang, and Y. Zhao, Journal of Physical Chemistry Letters **14**, 6990 – 6997 (2023).

[52]K. J. Tielrooij, J. C. W. Song, S. A. Jensen, A. Centeno, A. Pesquera, A. Zurutuza Elorza, M. Bonn, L. S. Levitov, and F. H. L. Koppens, Nature Phys. **9**, 248 (2013).

[53]M. Statz, V. D., X. Jiao, S. Schott, C. R. McNeill, D. Emin, H. Sirringhaus, and R. D. Pietro, Commun. Phys. **1**, 16 (2018).

[54]A. F. Kemper, O. Abdurazakov, and J. K. Freericks, Phys. Rev. X **8**, 041009 (2018).

[55]J. Young, T. Gong, P. Fauchet, and P. Kelly, Phys. Rev. B **50**, 2208 (1994).

[56]F. Rossi and T. Kuhn, Rev. Mod. Phys. **74**, 895 (2002).

[57]P. C. Becker, H. L. Fragnito, C. H. B. Cruz, L. R. Fork, J. E. Cunningham, J. E. Henry, and C. V. Shank, Phys. Rev. Lett. **61**, 1647 (1988).

[58]W. A. Hügel, M. F. Heinrich, M. Wegener, Q. T. Vu, L. Bányai, and H. Haug, Phys. Rev. Lett. **83**, 3313 (1999).

[59]R. Huber, F. Tauser, A. Brodschelm, M. Bichler, G. Abstreiter, and A. Leitenstorfer, Nature **414**, 286 (2001).

[60]J. Sjakste, N. Vast, G. Barbarino, M. Calandra, F. Mauri, J. Kanasaki, H. Tanimura, and K. Tanimura, Phys. Rev. B **97**, 064302 (2018).

[61]P. Allen, Phys. Rev. Lett. **59**, 1460 (1987).

[62]S. Ono, Phys. Rev. B **97**, 054310 (2018).

[63]Z. Chen, C. Giorgetti, J. Sjakste, R. Cabouat, V. Veniard, Z. Zhang, A. Taleb-Ibrahimi, E. Papalazarou, M. Marsi, A. Shukla, J. Peretti, and L. Perfetti, Phys. Rev. B **97**, 241201(R) (2018).

[64]T. Ichibayashi, S. Tanaka, J. Kanasaki, K. Tanimura, and T. Fauster, Phys. Rev. B **84**,

235210 (2011).

[65]M. Bernardi, D. Vigil-Fowler, J. Lischner, J. B. Neaton, and S. G. Louie, Phys. Rev. Lett. **112**, 257402 (2014).

[66]S. A. Sato, Computational Materials Science **194**, 110274 (2021).

[67]E. Runge and E. Gross, Phys. Rev. Lett. **52**, 997 (1984).

[68]G. Bertsch, J.-I. Iwata, A. Rubio, and K. Yabana, Phys. Rev. B **62**, 7998 (2000).

[69]S. A. Sato, K. Yabana, Y. Shinohara, T. Otobe, and G. F. Bertsch, Phys. Rev. B **89**, 064304 (2014).

[70]U. D. Giovannini, H. Hübener, and A. Rubio, Journal of Chemical Theory and Computation **13**, 265 (2017).

[71]C. Lian, M. Guan, S. Hu, J. Zhang, and S. Meng, Advanced Theory and Simulations **1**, 1800055 (2018).

[72]M. Qasim, M. S. Wismer, M. Agarwal, and V. S. Yakovlev, Phys. Rev. B **98**, 214304 (2018).

[73]R. R. Pela and C. Draxl, Electronic Structure **3**, 037001 (2021).

[74]T. Moitra, L. Konecny, M. Kadek, A. Rubio, and M. Repisky, The Journal of Physical Chemistry Letters **14**, 1714 (2023).

[75]E. P. Silaeva, E. Bevillon, R. Stoian, and J. P. Colombier, Phys. Rev. B **98**, 094306 (2018).

[76]K. Krieger, J. K. Dewhurst, P. Elliott, S. Sharma, and E. K. U. Gross, Journal of Chemical Theory and Computation **11**, 4870 (2015).

[77]A. Kononov, C.-W. Lee, T. P. dos Santos, B. Robinson, Y. Yao, Y. Yao, X. Andrade, A. D. Baczewski, E. Constantinescu, A. A. Correa, Y. Kanai, N. Modine, and A. Schleife, MRS Communications **12**, 1002 (2022).

[78]E. Perfetto and G. Stefanucci, Phys. Rev. A **91**, 033416 (2015).

[79]E. Perfetto, D. Sangalli, A. Marini, and G. Stefanucci, Phys. Rev. B **94**, 245303 (2016).

[80]D. Sangalli, E. Perfetto, and G. a. Stefanucci, Eur. Phys. J. B **91**, 171 (2018).

[81]A. Marini, E. Perfetto, and G. Stefanucci, Journal of Electron Spectroscopy and Related Phenomena **257**, 147189 (2022).

[82]E. Perfetto, Y. Pavlyukh, and G. Stefanucci, Phys. Rev. Lett. **128**, 016801 (2022).

[83]E. Perfetto and G. Stefanucci, Nano Letters , 7029 (2023).

[84]W. Miao and M. Wang, Phys. Rev. B **103**, 125412 (2021).

[85]D. Yadav, M. Trushin, and F. Pauly, Phys. Rev. Res. **2**, 043051 (2020).

[86]H. M. Van Driel, Phys. Rev. B **35**, 8166 (1987).

[87]V. C. Paingad, J. Kunc, M. Rejhon, I. Rychetský, I. Mohelský, M. Orlita, and P. Kužel, Advanced Functional Materials **31**, 2105763 (2021).

[88]R. Binder, D. Scott, A. E. Paul, M. Lindberg, K. Henneberger, and S. W. Koch, Phys. Rev. B **45**, 1107 (1992).

[89]L. Jiang and H.-L. Tsai, Journal of Heat Transfer-transactions of The Asme **127**, 1167 (2005).

[90]N. SINGH, International Journal of Modern Physics B **24**, 1141 (2010).

[91]W. H. Knox, D. S. Chemla, G. Livescu, J. E. Cunningham, and J. E. Henry, Phys. Rev. Lett. **61**, 1290 (1988).

[92]S. Sadasivam, M. Chan, and P. Darancet, Phys. Rev. Lett. **119**, 136602 (2017).

[93]J. Faure, J. Mauchain, E. Papalazarou, M. Marsi, D. Boschetto, I. Timrov, N. Vast, Y. Ohtsubo, B. Arnaud, and L. Perfetti, Phys. Rev. B **88**, 075120 (2013).

[94]W.-T. Hsu, Y.-L. Chen, C.-H. Chen, P.-S. Liu, T.-H. Hou, L.-J. Li, and W.-H. Chang, Nature Communications **6**, 8963 (2015).

[95]Molina-Sánchez, D. Sangalli, L. Wirtz, and A. Marini, Nano Letters **17**, 45494555 (2017).

[96]S. Xu, C. Si, Y. Li, B.-L. Gu, and W. Duan, Nano Letters **21**, 1785 – 1791 (2021).

[97]S. Bae, K. Matsumoto, H. Raebiger, K.-i. Shudo, Y.-H. Kim, S. Handegård, T. Nagao, M. Kitajima, Y. Sakai, X. Zhang, R. Vajtai, P. Ajayan, J. Kono, J. Takeda, and I. Katayama, Nature Communications **13**, 4279 (2022).

[98]X.-W. Zhang, K. Xie, E.-G. Wang, X.-Z. Li, and T. Cao, The Journal of Physical Chemistry Letters **15**, 7584 (2024), pMID: 39025480.

[99]V. Djurberg, S. Majdi, N. Suntornwipat, and J. Isberg, Materials for Quantum Technology **3**, 025001 (2023).

[100]J. Shah, B. Deveaud, T. C. Damen, W. T. Tsang, A. C. Gossard, and P. Lugli, Phys. Rev. Lett **59**, 2222 (1987).

[101]J. Sjakste, V. Tyuterev, and N. Vast, Applied Physics A **86**, 301 (2007).

[102]K. Tanimura, H. Tanimura, and J. Kanasaki, Physical Review B **106** (2022), 10.1103/PhysRevB.106.125204.

[103]I. Gierz, J. C. Petersen, M. Mitrano, C. Cacho, I. C. E. Turcu, E. Springate, A. Stöhr, A. Köhler, U. Starke, and A. Cavalleri, Nature Mater **12**, 1119 (2013).

[104]J. Reimann, K. Sumida, M. Kakoki, K. Kokh, O. Tereshchenko, A. Kimura, J. Güdde, and U. Höfer, Scientific Reports **13**, 5796 (2023).

[105]K. Kuroda, J. Reimann, J. Güdde, and U. Höfer, Phys. Rev. Lett. **116**, 076801 (2016).

[106]S. Kovalev, K.-J. Tielrooij, J.-C. Deinert, I. Ilyakov, N. Awari, M. Chen, A. Ponomaryov, M. Bawatna, T. V. A. G. de Oliveira, L. M. Eng, K. A. Kuznetsov, D. A. Safronenkov, G. K. Kitaeva, P. I. Kuznetsov, H. A. Hafez, D. Turchinovich, and M. Gensch, npj Quantum Mater. **6**, 84 (2021).

[107]D. Sangalli, Phys. Rev. Mater. **5**, 083803 (2021).

[108]F. Caruso, D. Novko, and C. Draxl, Phys. Rev. B **101**, 035128 (2020).

[109]S. Ponce, E. R. Margine, C. Verdi, and F. Giustino, Comp. Phys. Comm. **209**, 116 (2016).

[110]S. Poncé, F. Macheda, E. Margine, N. Marzari, N. Bonini, and F. Giustino, Phys. Rev. Research **3**, 043022 (2021).

[111]S. Ahmad, O. Daga, and W. Khokle, Phys. Stat. Sol. **40**, 631 (1970).

[112]V. P. Zhukov, P. M. Echenique, and E. V. Chulkov, Phys. Rev. B **82**, 094302 (2010).

[113]V. Tyuterev, J. Sjakste, and N. Vast, Phys. Rev. B **81**, 245212 (2010).

[114]J. L. Birman, M. Lax, and R. Loudon, Phys. Rev. **145**, 620 (1966).

[115]G. Marini, G. Marchese, G. Profeta, J. Sjakste, F. Macheda, N. Vast, F. Mauri, and M. Calandra, Comp. Phys. Comm. **295**, 108950 (2024).

[116]R. Sen, N. Vast, and J. Sjakste, Appl. Phys. Lett. **120**, 082101 (2022).

[117]M. V. Fischetti, P. Yoder, M. Khatami, G. Gaddemane, and L. V. de Put, Appl. Phys. Lett. **114**, 222104 (2019).

[118]A. Katz and R. Alfano, Appl. Phys. Lett. **53**, 1065 (1988).

[119]X. Gonze, Phys. Rev. A **52**, 1096 (1995).

[120]S. Baroni, S. de Gironcoli, A. D. Corso, and P. Giannozzi, Rev. Mod. Phys. **73**, 515 (2001).

[121]F. Mauri, O. Zakharov, S. de Gironcoli, S. Louie, and M. Cohen, Phys. Rev. Lett. **77**, 1151 (1996).

[122]S. Y. Savrasov, Phys. Rev. B **54**, 16470 (1996).

[123]M. Calandra, N. Vast, and F. Mauri, Phys. Rev. B **69**, 224505 (2004).

[124]F. Giustino, J. R. Yates, I. Souza, M. Cohen, and S. G. Louie, Phys. Rev. Lett. **98**, 047005 (2007).

[125]M. Calandra and F. Mauri, Phys. Rev. Lett. **101**, 016401 (2008).

[126]C. Brun, I.-P. Hong, F. Patthey, I. Y. Sklyadneva, R. Heid, P. M. Echenique, K. P. Bohnen, E. V. Chulkov, and W.-D. Schneider, Phys. Rev. Lett. **102**, 207002 (2009).

[127]M. Calandra and F. Mauri, Phys. Rev. Lett. **106**, 196406 (2011).

[128]J. Sjakste, V. Tyuterev, and N. Vast, Phys. Rev. B **74**, 235216 (2006).

[129]J. Sjakste, N. Vast, and V. Tyuterev, Phys. Rev. Lett. **99**, 236405 (2007).

[130]S. Baroni, P. Giannozzi, and A. Testa, Phys. Rev. Lett. **58**, 1861 (1987).

[131]F. Murphy-Armando and S. Fahy, Phys. Rev. B **78**, 035202 (2008).

[132]O. D. Restrepo, K. Varga, and S. T. Pantelides, Appl. Phys. Lett. **94**, 212103 (2009).

[133]Z. Wang, S. Wang, S. Obukhov, N. Vast, J. Sjakste, V. Tyuterev, and N. Mingo, Phys. Rev. B **83**, 205208 (2011).

[134]J. J. Zhou and M. Bernardi, Phys. Rev. B **94**, 201201 (2016).

[135]T.-H. Liu, J. Zhou, B. Liao, D. J. Singh, and G. Chen, Phys. Rev. B **95**, 075206 (2017).

[136]V. Tyuterev, S. Obukhov, N. Vast, and J. Sjakste, Phys. Rev. B **84**, 035201 (2011).

[137]N. Tandon, J. D. Albrecht, and L. R. Ram-Mohan, J. Appl. Phys. **118**, 045713 (2015).

[138]N. Tandon, J. Albrecht, and S. Badescu, Journal of Electronic Materials **53**, 1161 – 1168 (2024).

[139]F. Giustino, S. Louie, and M. Cohen, Phys. Rev. Lett. **105**, 265501 (2010).

[140]E. Cannuccia and A. Marini, Phys. Rev. Lett. **107**, 255501 (2011).

[141]X. Gonze, P. Boulanger, and M. Côté, Ann. Phys. (Berlin) **523**, 168 (2011).

[142]S. Poncé, Y. Gillet, J. L. Janssen, A. Marini, M. Verstraete, and X. Gonze, J. Chem. Phys. **143**, 102813 (2015).

[143]G. Antonius, S. Poncé, E. Lantagne-Heurtebise, G. Auclair, X. Gonze, and M. Côté, Phys. Rev. B **92**, 085137 (2015).

[144]J. P. Nery and P. B. Allen, Phys. Rev. B **94**, 115135 (2016).

[145]E. Kioupakis, P. Rinke, A. Schleife, F. Bechstedt, and C. G. V. de Walle, Phys. Rev. B **81**, 241201(R) (2010).

[146]J. Noffsinger, E. Kioupakis, C. V. de Walle, S. Louie, and M. Cohen, Phys. Rev. Lett. **108**, 167402 (2012).

[147]B. Liao, B. Qiu, J. Zhou, S. Huberman, K. Esfarjani, and G. Chen, Phys. Rev. Lett. **114**, 115901 (2015).

[148]H.-Y. Chen, D. Sangalli, and M. Bernardi, Phys. Rev. Lett. **125**, 107401 (2020).

[149]M. R. Filip, J. B. Haber, and J. B. Neaton, Phys. Rev. Lett. **127**, 067401 (2021).

[150]Z. Dai, C. Lian, J. Lafuente-Bartolome, and F. Giustino, Phys. Rev. Lett. **132**, 036902 (2024).

[151]F. Murphy-Armando, G. Fagas, and J. C. Greer, Nano Letters **10**, 869 (2010).

[152]F. Murphy-Armando and S. Fahy, J. Appl. Phys. **109**, 113703 (2011).

[153]P. Han and G. Bester, Phys. Rev. B **85**, 234422 (2012).

[154]M. P. Vaughan, F. Murphy-Armando, and S. Fahy, Phys. Rev. B **85**, 165209 (2012).

[155]L. Waldecker, R. Bertoni, H. Hubener, T. Brumme, Vasileiadis, D. Zahn, A. Rubio, and R. Ernstorfer, Phys. Rev. Lett. **119**, 036803 (2017).

[156]T. Sohier, D. Campi, N. Marzari, and M. Gibertini, Phys. Rev. Mat. **2**, 114010 (2018).

[157]T. Sohier, M. Gibertini, D. Campi, G. Pizzi, and N. Marzari, Nano Lett. **19**, 3723 (2019).

[158]M. R. Filip and L. Leppert, Electronic Structure **6**, 033002 (2024).

[159]P. Giannozzi, O. Andreussi, T. Brumme, O. Bunau, M. B. Nardelli, M. Calandra, R. Car, C. Cavazzoni, D. Ceresoli, M. Cococcioni, N. Colonna, I. Carnimeo, A. D. Corso, S. de Gironcoli, P. Delugas, R. A. D. J. A. Ferretti, A. Floris, G. Fratesi, G. Fugallo, R. Gebauer, U. Gerstmann, F. Giustino, T. Gorni, J. Jia, M. Kawamura, H.-Y. Ko, A. Kokalj, E. Küçükbenli, M. Lazzeri, M. Marsili, N. Marzari, F. Mauri, N. L. Nguyen, H.-V. Nguyen, A. O. de-la Roza, L. Paulatto, S. Poncé, D. Rocca, R. Sabatini, B. Santra, M. Schlipf, A. P. Seitsonen, A. Smogunov, I. Timrov, T. Thonhauser, P. Umari, N. Vast, X. Wu, and S. Baroni, J. Phys.: Condens. Matter **29**, 465901 (2017).

[160]X. Gonze, B. Amadon, G. Antonius, F. Arnardi, L. Baguet, J.-M. Beuken, J. Bieder, F. Bottin, J. Bouchet, E. Bousquet, N. Brouwer, F. Bruneval, G. Brunin, T. Cavignac, J.-B. Charraud, W. Chen, M. Côté, S. Cottenier, J. Denier, G. Geneste, P. Ghosez, M. Giantomassi, Y. Gillet, O. Gingras, D. R. Hamann, G. Hautier, X. He, N. Helbig, N. Holzwarth, Y. Jia, F. Jollet, W. Lafargue-Dit-Hauret, K. Lejaeghere, M. A. Marques, A. Martin, C. Martins, H. P. Miranda, F. Naccarato, K. Persson, G. Petretto, V. Planes, Y. Pouillon, S. Prokhorenko, F. Ricci, G.-M. Rignanese, A. H. Romero, M. M. Schmitt, M. Torrent, M. J. van Setten, B. Van Troeye, M. J. Verstraete, G. Zérah, and J. W. Zwanziger, Computer Physics Communications **248**, 107042 (2020).

[161]G. Kresse and D. Joubert, Phys. Rev. B **59**, 1758 (1999).

[162]J.-J. Zhou, J. Park, I. Timrov, A. Floris, M. Cococcioni, N. Marzari, and M. Bernardi, Phys. Rev. Lett. **127**, 126404 (2021).

[163]G. Antonius, S. Poncé, P. Boulanger, M. Côté, and X. Gonze, Phys. Rev. Lett. **112**, 215501 (2014).

[164]B. Monserrat, Phys. Rev. B **93**, 100301(R) (2016).

[165]F. Karsai, M. Engel, E. Flage-Larsen, and G. Kresse, New J. Phys. **20**, 123008 (2018).

[166]M. Engel, M. Marsman, C. Franchini, and G. Kresse, Phys. Rev. B **101**, 184302 (2020).

[167]M. Engel, H. Miranda, L. Chaput, A. Togo, C. Verdi, M. Marsman, and G. Kresse, Phys. Rev. B **106**, 094316 (2022).

[168]A. Miglio, V. Brousseau-Couture, E. Godbout, G. Antonius, Y.-H. Chan, S. G. Louie, M. Côté, M. Giantomassi, and X. Gonze, npj Computational Materials **6**, 167 (2020).

[169]N. Marzari, A. A. Mostofi, J. R. Yates, I. Souza, and D. Vanderbilt, Rev. Mod. Phys. **84**, 1419 (2012).

[170]J.-J. Zhou, J. Park, I.-T. Lu, I. Maliyov, X. Tong, and M. Bernardi, Computer Physics Communications **264**, 107970 (2021).

[171]M. Calandra, G. Profeta, and F. Mauri, Phys. Rev. B **82**, 165111 (2010).

[172]C. Verdi and F. Giustino, Phys. Rev. Lett. **115**, 176401 (2015).

[173]P. Vogl, Phys. Rev. B **13**, 694 (1976).

[174]L. Agapito and M. Bernardi, Phys. Rev. B **97**, 235146 (2018).

[175]G. Brunin, H. P. C. Miranda, M. Giantomassi, M. Royo, M. Stengel, M. J. Verstraete, X. Gonze, G.-M. Rignanese, and G. Hautier, Phys. Rev. B **102**, 094308 (2020).

[176]N. E. Lee, J. J. Zhou, H. Y. Chen, and M. Bernardi, Nature Communications **11**, 1607 (2020).

[177]P. S. Cheng, J. Sun, S.-N. Sun, A. Y. Choi, and A. J. Minnich, Phys. Rev. B **106**, 245201 (2022).

[178]B. Hatanpää, A. Y. Choi, P. S. Cheng, and A. J. Minnich, Phys. Rev. B **107**, L041110 (2023).

[179]F. Murphy-Armando and S. Fahy, Phys. Rev. B **86**, 079903 (2012).

[180]S. Poncé, E. Margine, and F. Giustino, Phys. Rev. B **97**, 121201 (2018).

[181]S. Poncé, M. Royo, M. Gibertini, N. Marzari, and M. Stengel, Phys. Rev. Lett. **13**, 166301 (2023).

[182]D. S. Catherall and A. J. Minnich, Phys. Rev. B **107**, 035201 (2023).

[183]B. Dongre, J. Carrete, S. Wen, J. Ma, W. Li, N. Mingo, and G. K. H. Madsen, J. Mater. Chem. A **8**, 1273 (2020).

[184]A. M. Saitta, M. Lazzeri, M. Calandra, and F. Mauri, Phys. Rev. Lett. **100**, 226401 (2008).

[185]F. Herziger, M. Calandra, P. Gava, P. May, M. Lazzeri, F. Mauri, and J. Maultzsch, Phys. Rev. Lett. **113**, 187401 (2014).

[186]L. Graziotto, F. Macheda, T. Sohier, M. Calandra, and F. Mauri, Phys. Rev. B **109**, 075420 (2024).

[187]M. Fiorentini and N. Bonini, Phys. Rev. B **94**, 085204 (2016).

[188]N. Protik, C. Li, M. Pruneda, D. Broido, and P. Ordejon, npj Comput. Mater. **8**, 28 (2022).

[189]G. Marini, M. Calandra, and P. Cudazzo, Nano Letters **24**, 6017 (2024), pMID: 38723148.

[190]D. Dangić, L. Monacelli, R. Bianco, F. Mauri, and I. Errea, Communications Physics **7**, 150 (2024).

[191]A. Sanna, T. F. T. Cerqueira, Y.-W. Fang, I. Errea, A. Ludwig, and M. A. L. Marques, npj Computational Materials **10**, 44 (2024).

[192]L. Monacelli, R. Bianco, M. Cherubini, M. Calandra, I. Errea, and F. Mauri, Journal of Physics: Condensed Matter **33**, 363001 (2021).

[193]I. Pallikara, P. Kayastha, J. M. Skelton, and L. D. Whalley, Electronic Structure **4**, 033002 (2022).

[194]M. Lazzeri and F. Mauri, Phys. Rev. Lett. **97**, 266407 (2006).

[195]S. Tan, A. Argondizzo, C. Wang, X. Cui, and H. Petek, Phys. Rev. X **7**, 011004 (2017).

[196]N. Girotto, F. Caruso, and D. Novko, The Journal of Physical Chemistry C **127**, 16515 (2023).

[197]J.-J. Zhou and M. Bernardi, Phys. Rev. Res. **1**, 033138 (2019).

[198]W. H. Sio, C. Verdi, S. Poncé, and F. Giustino, Phys. Rev. Lett. **122**, 246403 (2019).

[199]B. Hatanpää and A. J. Minnich, Phys. Rev. B **109**, 235201 (2024).

[200]T. Sohier, M. Calandra, and F. Mauri, Phys. Rev. B **94**, 085415 (2016).

[201]T. Sohier, M. Calandra, and F. Mauri, Phys. Rev. B **96**, 075448 (2017).

[202]J. Berges, N. Girotto, T. Wehling, N. Marzari, and S. Poncé, Phys. Rev. X **13**, 041009 (2023).

[203]J. Park, J.-J. Zhou, and M. Bernardi, Phys. Rev. B **101**, 045202 (2020).

[204]J. Xu, A. Habib, S. Kumar, F. Wu, R. Sundararaman, and Y. Ping, Nature Commun. **11**, 2780 (2020).

[205]J. Park, J.-J. Zhou, Y. Luo, and M. Bernardi, Phys. Rev. Lett. **129**, 197201 (2022).

[206]Z. P. Yin, A. Kutepov, and G. Kotliar, Phys. Rev. X **3**, 021011 (2013).

[207]J. Yu, C. J. Ciccarino, R. Bianco, I. Errea, P. Narang, and B. A. Bernevig, Nature Physics **20**, 1262 (2024).

[208]Z. Li, P. Graziosi, and N. Neophytou, Phys. Rev. B **104**, 195201 (2021).

[209]D. Dangić, S. Fahy, and I. Savić, Npj Comput. Mater. **6**, 195 (2020).

[210]Y. Huang, J. D. Querales-Flores, S. W. Teitelbaum, J. Cao, T. Henighan, H. Liu, M. Jiang, G. De la Peña, V. Krapivin, J. Haber, T. Sato, M. Chollet, D. Zhu, T. Katayama, R. Power, M. Allen, C. R. Rotundu, T. P. Bailey, C. Uher, M. Trigo, P. S. Kirchmann, E. D. Murray, Z.-X. Shen, I. Savić, S. Fahy, J. A. Sobota, and D. A. Reis, Phys. Rev. X **13**, 041050 (2023).

[211]N. Neophytou, P. Priyadarshi, Z. Li, and P. Graziosi, Journal of Computational Electronics **22**, 1264 (2023).

[212]N. Vast, J. Sjakste, G. Kané, and V. Trinité, *Electrons, phonons, and their coupling within the density functional theory*, edited by P. Dollfus and F. Triozon, Simulation of transport in nanodevices, Vol. 1 (ISTE Ltd, 2016) p. (2016).

[213]S. Sarkar, I.-W. Un, Y. Sivan, and Y. Dubi, New Journal of Physics **24** (2022), 10.1088/1367-2630/ac6688.

[214]H. Maris, *Physical Acoustics*, edited by W. P. Mason, Vol. 8 (Academic Press, New York, 1971) pp. 279–345.

[215]A. Debernardi, S. Baroni, and E. Molinari, Phys. Rev. Lett. **75**, 1819 (1995).

[216]N. Mingo, D. Hauser, N. Kobayashi, M. Plissonnier, and A. Shakouri, Nano Lett. **9**, 711 (2009).

[217]K. Esfarjani, G. Chen, and H. Stokes, Phys. Rev. B **84**, 085205 (2011).

[218]L. Chaput, Phys. Rev. Lett. **110**, 265506 (2013).

[219]M. Markov, J. Sjakste, G. Fugallo, L. Paulatto, M. Lazzeri, F. Mauri, and N. Vast, Phys. Rev. B **93**, 064301 (2016).

[220]M. Markov, J. Sjakste, N. Vast, R. Legrand, B. Perrin, and L. Paulatto, Phys. Rev. B **98**, 245201 (2018).

[221]P. D. Thacher, Phys. Rev. **156**, 975 (1967).

[222]V. I. Ozhogin, A. V. Inyushkin, A. N. Taldenkov, A. V. Tikhomirov, and G. E. Popov, JETP Lett. **63**, 490 (1996).

[223]A. P. Zhernov and A. V. Inyushkin, Phys. Usp. **45**, 527 (2002).

[224]L. Lindsay, Nanoscale and Microscale Thermophysical Engineering **20**, 67 (2016).

[225]A. V. Inyushkin, A. N. Taldenkov, A. M. Gibin, A. V. Gusev, and H.-J. Pohl, Phys. Status Solidi C **1**, 2995 (2004).

[226]A. V. Inyushkin, N. V. Abrosimov, A. N. Taldenkov, J. W. Ager, E. E. Haller, H. Riemann, H.-J. Pohl, and P. Becker, J. Appl. Phys. **123**, 095112 (2018).

[227]Z. Ding, K. Chen, B. Song, J. Shin, A. Maznev, K. Nelson, and G. Chen, Nat. Comm. **13**, 285 (2022).

[228]J. Zhou, B. Liao, B. Qiu, S. Huberman, K. Esfarjani, M. Dresselhaus, and G. Chen, Proc. Natl. Acad. Sci. U. S. A. **112**, 14777 (2015).

[229]B. Liao, A. A. Maznev, K. A. Nelson, and G. Chen, Nat Commun **7**, 13174 (2016).

[230]V. Shokeen, M. Heber, D. Kutnyakhov, X. Wang, A. Yaroslavtsev, P. Maldonado, M. Berritta, N. Wind, L. Wenthaus, F. Pressacco, C.-H. Min, M. Nissen, S. K. Mahatha, S. Dziarzhytski, P. M. Oppeneer, K. Rossnagel, H.-J. Elmers, G. Schönhense, and H. A. Dürr, Science Advances **10**, eadj2407 (2024).

[231]C. Herring, Phys. Rev. **96**, 1163 (1954).

[232]N. Protik and B. Kozinsky, Phys. Rev. B **102**, 245202 (2020).

[233]Q. Xu, J. Zhou, T. Liu, and G. Chen, Phys. Rev. Applied **16**, 064052 (2021).

[234]L. Challis, *Electron-Phonon Interactions in Low-Dimensional Structures* (Oxford University Press, 2003).

[235]W. Cai, M. C. Marchetti, and M. Lax, Phys. Rev. B **37**, 2636 (1988).

[236]R. Gupta, N. Balkan, and B. K. Ridley, Phys. Rev. B **46**, 7745 (1992).

[237]X. Zhou, W. W. Rühle, P. Schullatz, P. Kocevar, H. M. van Driel, and K. Ploog, Semicond. Sci. Technol. **9**, 704 (1994).

[238]F. Sekiguchi, H. Hirori, G. Yumoto, A. Shimazaki, T. Nakamura, A. Wakamiya, and Y. Kanemitsu, Phys. Rev. Lett. **126**, 077401 (2021).

[239]O. Herrfurth, E. Krüger, S. Blaurock, H. Krautscheid, and M. Grundmann, Journal of Physics: Condensed Matter **33**, 205701 (2021).

[240]E. N. Bogachek, I. O. Kulik, and A. G. Shkorbatov, Journal of Physics: Condensed Matter **3**, 8877 (1991).

[241]D. Vasileska, K. Raleva, and S. Goodnick, J. Comput. Electron **7**, 66 (2008).

[242]V. F. Gantmakher, Reports on Progress in Physics **37**, 317 (1974).

[243]H. Zeiger, J. Vidal, T. Cheng, E. Ippen, G. Dresselhaus, and M. Dresselhaus, Phys. Rev. B **45**, 768 (1992).

[244]A. V. Kuznetsov and C. J. Stanton, Phys. Rev. Lett. **73**, 3243 (1994).

[245]G. Garrett, T. Albrecht, J. Whitaker, and R. Merlin, Phys. Rev. Lett. **77**, 3661 (1996).

[246]R. Merlin, Solid State Commun. **102**, 207 (1997).

[247]T. E. Stevens, J. Kuhl, and R. Merlin, Phys. Rev. B **65**, 144304 (2002).

[248]Y. Giret, A. Gellé, and B. Arnaud, Phys. Rev. Lett. **106**, 155503 (2011).

[249]Y. Shinohara, A. Sato, K. Yabana, J.-I. Iwata, T. Otobe, and G. Bertsch, J. Chem. Phys. **137**, 22A527 (2012).

[250]E. Papalazarou, J. Faure, J. Mauchain, M. Marsi, A. Taleb-Ibrahimi, I. Reshetnyak, A. van Roekeghem, I. Timrov, N. Vast, B. Arnaud, and L. Perfetti, Phys. Rev. Let. **108**, 256808 (2012).

[251]E. Murray and S. Fahy, Phys. Rev. Lett. **114**, 055502 (2015).

[252]Y. Kayanuma and K. Nakamura1, Phys. Rev. B **95**, 104302 (2017).

[253]A. Othonos, H. M. van Driel, J. F. Young, and P. J. Kelly, Phys. Rev. B **43**, 6682 (1991).

[254]J. J. Letcher, K. Kang, D. G. Cahill, and D. D. Dlott, Applied Physics Letters **90**, 252104 (2007), https://pubs.aip.org/aip/apl/article-pdf/doi/10.1063/1.2749728/13959780/252104_1_online.pdf.

[255]H. Yan, D. Song, K. F. Mak, I. Chatzakis, J. Maultzsch, and T. F. Heinz, Phys. Rev. B **80**, 121403 (2009).

[256]H.Brooks and C.Herring, Phys. Rev. **83**, 879 (1951).

[257]S. S. Li and W. R. Thurber, Solid-State Electronics **20**, 609 (1977).

[258]J. Leveillee, X. Zhang, E. Kioupakis, and F. Giustino, Phys. Rev. B **107**, 125207 (2023).

[259]P. Yu and M. Cardona, *Fundamentals of Semiconductors* (Springer-Verlag, Berlin New York, 2001).

[260]M. V. Fischetti and S. E. Laux, Phys. Rev. B **38**, 9721 (1988).

[261]C. Jacoboni and L. Reggiani, Rev. Mod. Phys. **55**, 645 (1983).

[262]S. Zollner, S. Gopalan, and M. Cardona, Appl. Phys. Lett. **54**, 614 (1989).

[263]V. Djurberg, S. Majdi, N. Suntornwipat, and J. Isberg, Phys. Rev. B **106**, 045205 (2022).

[264]Z. He, A.-A. Sun, and S.-P. Gao, Phys. Rev. B **108**, 165108 (2023).

[265]O. D. Restrepo, K. E. Krymowski, J. Goldberger, and W. Windl, New Journal of Physics **16**, 105009 (2014).

[266]I.-T. Lu, J.-J. Zhou, and M. Bernardi, Phys. Rev. Mater. **3**, 033804 (2019).

[267]G. Fugallo, M. Lazzeri, L. Paulatto, and F. Mauri, Phys. Rev. B **88**, 045430 (2013).

[268]S. Tamura, Phys. Re. B **27**, 858 (1983).

[269]M. Omini and A. Sparavigna, Il Nuovo Cimento D **19**, 1537 (1997).

[270]A. Sparavigna, Phys. Rev. B **65**, 064305 (2002).

[271]J. Sjakste, M. Markov, R. Sen, G. Fugallo, L. Paulatto, and N. Vast, Nano Express **5**, 035018 (2024).

[272]A. Katre, J. Carrete, B. Dongre, G. K. H. Madsen, and N. Mingo, Phys. Rev. Lett. **119**, 075902 (2017).

[273]L. Malakkal, A. Katre, S. Zhou, C. Jiang, D. H. Hurley, C. A. Marianetti, and M. Khafizov, Phys. Rev. Mater. **8**, 025401 (2024).

[274]K. Ashida, M. Inoue, J. Shirafuji, and Y. Inuishi, J. Phys. Soc. Jpn. **37**, 408 (1974).

[275]M. Wais, K. Held, and M. Battiato, Computer Physics Communications **264**, 107877 (2021).

[276]X. Tong and M. Bernardi, Phys. Rev. Res. **3**, 023072 (2021).

[277]H. Tanimura and K. Tanimura, Phys. Rev. B **102**, 045204 (2020).

[278]F. Stern, Phys. Rev. Lett. **18**, 546 (1967).

[279](), specimens were cut from p-type Ge(111) wafers of 0.5 mm thickness and were then cleaned in an ultra-high vacuum. The *s*-polarised pump laser pulses of 1.55 eV and 100 fs were generated by Ti:sapphire laser oscillator. A portion of the fundamental light was used to generate the 3rd harmonic pulses (4.65 eV, *p*-pol.) to probe the photoexcited electrons. The time delay between the two laser pulses was changed in a range from -5 to 5 ps by using a computer-controlled delay stage. The hemispherical analyzer was operated in an angle-resolved lens mode, and the energy resolution was set to 50 meV. Photoelectron images were recorded as a function of kinetic energy and emission angle of photoelectrons, at respective time delays.

[280](), germanium was described within the LDA approximation, with a cutoff energy of 60 Ry and a 12x12x12 Γ-centered **k**-point grid. The lattice parameter of 10.696 a.u.[136] was used in all the calculations with the Quantum ESPRESSO package[159]. The Wannierization parameters used for the Wannier90 code[355] were as follows: 8 Wannier functions were constructed from 10 initial Bloch states, using atom-centered sp^3 projections as the initial guess. A disentanglement window of 17 eV and a frozen window of 12.203 eV were applied,

along with a 16 × 16 × 16 Γ-centered **k**-point grid. Disentanglement convergence was achieved within 109 iterations, with a tolerance of 10^{-12} Å^2, while the spread minimization reached a tolerance of 10^{-10} Å^2 after 200 iterations. The total spread for all eight Wannier functions was 33.45 Å^2. For the interpolation of the electron-phonon matrix elements within the EPW code[109], we used the above parameters and a 8x8x8 **q**-point grid.

[281]V. P. Zhukov, V. G. Tyuterev, E. V. Chulkov, and P. M. Echenique, J. App .Phys. **120**, 085708 (2016).

[282]M. Kaganov, I. Lifshitz, and L. Tanatarov, Sov Phys JETP **4**, 173 (1957).

[283]S. Anisimov, B. Kapeliovich, and T. Perel'man, Sov Phys JETP **39**, 375 (1973).

[284]P. B. Corkum, F. Brunel, N. K. Sherman, and T. Srinivasan-Rao, Phys. Rev. Lett. **61**, 2886 (1988).

[285]S. D. Brorson, A. Kazeroonian, J. S. Moodera, D. W. Face, T. K. Cheng, E. P. Ippen, M. S. Dresselhaus, and G. Dresselhaus, Phys. Rev. Lett. **64**, 2172 (1990).

[286]I. Klett and B. Rethfeld, Phys. Rev. B **98**, 144306 (2018).

[287]D.-Q. Xian and X.-H. Li, Thermal Science **21**, 1777 – 1782 (2017).

[288]S. Ono and T. Suemoto, Phys. Rev. B **102**, 024308 (2020).

[289]Z. Lu, A. Vallabhaneni, B. Cao, and X. Ruan, Phys. Rev. B **98**, 134309 (2018).

[290]S. M. O'Mahony, F. Murphy-Armando, E. D. Murray, J. D. Querales-Flores, I. Savić, and S. Fahy, Phys. Rev. Lett. **123**, 087401 (2019).

[291]M. Trigo, M. Fuchs, J. Chen, M. P. Jiang, M. Cammarata, S. Fahy, D. M. Fritz, K. Gaffney, S. Ghimire, A. Higginbotham, S. L. Johnson, M. E. Kozina, J. Larsson, H. Lemke, A. M. Lindenberg, G. Ndabashimiye, F. Quirin, K. Sokolowski-Tinten, C. Uher, G. Wang, J. S. Wark, D. Zhu, and D. A. Reis, Nature Physics **9**, 790 (2013).

[292]D. Zhu, A. Robert, T. Henighan, H. T. Lemke, M. Chollet, J. M. Glownia, D. A. Reis, and M. Trigo, Phys. Rev. B **92**, 054303 (2015).

[293]L. Waldecker, R. Bertoni, R. Ernstorfer, and J. Vorberger, Phys. Rev. X **6**, 021003 (2016).

[294]B. F. E. Curchod and T. J. Martínez, Chemical Reviews **118**, 3305 (2018).

[295]A. V. Akimov and O. V. Prezhdo, Journal of Chemical Theory and Computation **10**, 789 (2014).

[296]X. Zhou, M. V. Tokina, J. A. Tomko, J. L. Braun, P. E. Hopkins, and O. V. Prezhdo, The Journal of Chemical Physics **150**, 184701 (2019), https://pubs.aip.org/aip/jcp/article-pdf/doi/10.1063/1.5096901/13944667/184701_1_online.pdf.

[297]H. Nagata, T. Shinriki, K. Shima, M. Tamai, and E. Min Haga, Journal of Vacuum Science and Technology A **17**, 1018 (1999).

[298]S. Huang, M. Jiao, X. Wang, and X. He, Crystals **12**, 648 (2022).

[299]H. Bao, B. F. Habenicht, O. V. Prezhdo, and X. Ruan, Phys. Rev. B **79**, 235306 (2009).

[300]C. Zhao, Q. Zheng, and J. Zhao, Fundamental Research **2**, 506 (2022).

[301]H. Lu, R. Long, and W.-H. Fang, Journal of the American Chemical Society **145**, 25887 (2023).

[302]K. Hess, Physical Review B **12**, 2265 (1975).

[303]D. K. Ferry and J. R. Barker, Physical Review B **36**, 6018 (1987).

[304]L. Rota, P. Lugli, T. Elsaesser, and J. Shah, Phys. Rev. B **47**, 4226 (1993).

[305]T. Thu Trang Nghiêm, J. Saint-Martin, and P. Dollfus, Journal of Applied Physics **116** (2014), 10.1063/1.4893646.

[306]T. T. T. Nghiêm, J. Saint-Martin, and P. Dollfus, Journal of Computational Electronics **15**, 3 (2016).

[307]N. Izitounene, N. D. Le, B. Davier, P. Dollfus, L. Paulatto, and J. Saint-Martin, Crystal Research and Technology **57**, 2200017 (2022).

[308]B. Davier, P. Dollfus, N. Le, S. Volz, J. Shiomi, and J. Saint-Martin, International Journal of Heat and Mass Transfer **183**, 122056 (2022).

[309]J. Park, M. Pala, and J. Saint-Matin, in *2023 International Conference on Simulation of Semiconductor Processes and Devices (SISPAD)* (IEEE, 2023) pp. 21–24.

[310]P. Lugli and D. K. Ferry, Physical Review B **41**, 12659 (1990).

[311]L. Tirinoi, M. Weber, K. Brennana, E. Bellotti, and M. Goano, J. Appl. Phys. **94**, 423 (2003).

[312]H. Albuquerque, A. de Oliveira, G. Ribeiro, R. da Silva, W. Rodrigues, M. Moreira, and R. Rubinger, J. Appl. Phys. **93**, 1647 (2003).

[313]I. Pappas, A. Hatzopoulos, D. Tassis, N. Arpatzanis, S. Siskos, C. Dimitriadisa, and G. Kamarinos, J. Appl. Phys. **100**, 064506 (2006).

[314]P. Rodin, U. Ebert, A. Minarsky, and I. Grekhov, J. Appl. Phys. **102**, 034508 (2007).

[315]S. Chen and G. Wang, J. Appl. Phys. **103**, 023703 (2008).

[316]P. Lugli, P. Bordone, L. Reggiani, M. Rieger, P. Kocevar, and S. M. Goodnick, Phys. Rev. B **39**, 7852 (1989).

[317]V. V. Mitin, V. A. Kochelap, and M. A. Stroscio, Physical Review B **74**, 165305 (2006).

[318]M. Moresco, F. Bertazzi, and E. Bellotti, IEEE Journal of Quantum Electronics **47**, 447 (2011).

[319]D. Dolgos, H. Meier, A. Schenk, and B. Witzigmann, Journal of Applied Physics **110**, 084507 (2011).

[320]A. Srivastava, P. Srivastava, A. Srivastava, and P. K. Saxena, Scientific Reports **13**, 5630 (2023).

[321]J. Briones, H. C. Schneider, and B. Rethfeld, Journal of Physics Communications **6**, 035001 (2022).

[322]E. Tea, H. Hamzeh, and F. Aniel, J. Appl. Phys. **110**, 113108 (2011).

[323]D. O. Nielsen and M. V. Fischetti, Applied Physics Letters **123**, 252107 (2023), https://pubs.aip.org/aip/apl/article-pdf/doi/10.1063/5.0186802/18267274/252107_1_5.0186802.pdf.

[324]S. Gopalan, S. Mansoori, M. Van de Put, G. Gaddemane, and M. Fischetti, Journal of Computational Electronics **22**, 1240 (2023).

[325]Y. Zou, H. Esmaielpour, D. Suchet, J.-F. Guillemoles, and S. M. Goodnick, Scientific Reports **13**, 5601 (2023).

[326]E. Conwell, "High field transport in semiconductors," (Academic press, New York, 1967).

[327]E. E. Mendez, W. I. Wang, and L. L. Chang, Physical Review B **38**, 9721 (1988).

[328]J. Sjakste, I. Timrov, P. Gava, N. Mingo, and N. Vast, in *Annual Review of Heat Transfer*, Vol. 17 (Begell House Inc., Danbury, CT, USA, 2014) p. 333.

[329]T. T. NGHIÊM, V. Aubry-Fortuna, C. Chassat, A. Bosseboeuf, and P. Dollfus, Modern Physics Letters B **25**, 995 (2011).

[330]M. V. Fischetti, N. Sano, S. E. Laux, and K. Natori, Journal of Technology Computer Aided Design TCAD , 1 (1996).

[331]K. Rupp, C. Jungemann, S.-M. Hong, M. Bina, T. Grasser, and A. Jüngel, Journal of Computational Electronics **15**, 939 (2016).

[332]N. Fitzer, A. Kuligk, R. Redmer, M. Städele, S. M. Goodnick, and W. Schattke, Phys. Rev. B **67**, 201201 (2003).

[333]H. Ehrenreich and M. H. Cohen, Proceedings of SPIE **3179**, 114 (1997).

[334]J. Sun and A. J. Minnich, Phys. Rev. B **107**, 205201 (2023).

[335]T. Ghosh, S. Aharon, L. Etgar, and S. Ruhman, J. Am. Chem. Soc. **139**, 18262 (2017).

[336]S. Gopalan, G. Gaddemane, M. L. Van de Put, and M. V. Fischetti, Materials **12** (2019),

10.3390/ma12244210.

[337]P. Dollfus, C. Bru, and P. Hesto, J. App. Phys. **73**, 804 (1993).

[338]V. Aubry-Fortuna and P. Dollfus, J. Appl. Phys. **108**, 123706 (2010).

[339]M. A. Littlejohn, J. R. Hauser, and T. H. Glisson, J. Appl. Phys. **48**, 4587 (1977).

[340]D. Querlioz and P. Dollfus, *The Wigner Monte Carlo Method for Nanoelectronic Devices – A particle description of quantum transport and decoherence* (ISTE, London and Wiley, Hoboken, NJ, 2010).

[341]L. Shifren, C. Ringhofer, and D. K. Ferry, IEEE Trans. Electron Devices **50**, 769 (2003).

[342]M. Nedjalkov, D. Querlioz, P. Dollfus, and H. Kosina, in *Nano-Electronic Devices: Semiclassical and Quantum Transport Modeling*, edited by D. Vasileska and S. Goodnick (Springer, New York, Dordrecht, Heidelberg and London, 2011) pp. 289–358.

[343]D. Querlioz, J. Saint-Martin, A. Bournel, and P. Dollfus, Physical Review B **78**, 165306 (2008).

[344]D. Querlioz, J. Saint-Martin, V. N. Do, A. Bournel, and P. Dollfus, IEEE Trans. Nanotechnol. **5**, 737 (2006).

[345]D. Querlioz, J. Saint-Martin, K. Huet, A. Bournel, V. Aubry-Fortuna, C. Chassat, S. Galdin-Retailleau, and P. Dollfus, IEEE Trans. Electron Devices **54**, 2232 (2007).

[346]J. M. Sellier and I. Dimov, Journal of Computational Physics **280**, 287 (2015).

[347]J. M. Sellier, Physica A **496(C)**, 62 (2018).

[348]M. Benam, M. Ballicchia, J. Weinbub, S. Selberherr, and M. Nedjalkov, Journal of Computational Electronics **20**, 775 (2021).

[349]Y. Srivastava and A. Jain, Journal of Applied Physics **134**, 225101 (2023).

[350]Y. Luo, D. Desai, B. K. Chang, J. Park, and M. Bernardi, Phys. Rev. X **14**, 021023 (2024).

[351]V.-A. Ha and F. Giustino, npj Computational Materials **10**, 229 (2024).

[352]X. Gong, S. G. Louie, W. Duan, and Y. Xu, Nature Computational Science **4**, 752 (2024).

[353]H. Li, Z. Tang, J. Fu, W.-H. Dong, N. Zou, X. Gong, W. Duan, and Y. Xu, Phys. Rev. Lett. **132**, 096401 (2024).

[354]G. Stefanucci and E. Perfetto, SciPost Phys. **16**, 073 (2024).

[355]G. Pizzi, V. Vitale, R. Arita, S. Blugel, F. Freimuth, G. Géranton, M. Gibertini, D. Gresch, C. Johnson, T. Koretsune, J. Ibañez-Azpiroz, H. Lee, J. M. Lihm, D. Marchand, A. Marrazzo, Y. Mokrousov, J. I. Mustafa, Y. Nohara, Y. Nomura, L. Paulatto,

S. Poncé, T. Ponweiser, J. Qiao, F. Thole, S. S. Tsirkin, M. Wierzbowska, N. Marzari, D. Vanderbilt, I. Souza, A. A. Mostofi, and J. R. Yates, J. Phys.: Condens. Matter **32**, 165902 (2020).